2017-07-01

Acylation of Superoxide Dismutase 1 (SOD1) at K122 Alters SOD1 Localization and SOD1-Mediated Inhibition of Mitochondrial Respiration

Nathan William Rodriguez
Brigham Young University

Acylation of Superoxide Dismutase 1 (SOD1) at K122 Alters SOD1 Localization and SOD1-Mediated Inhibition of Mitochondrial Respiration

Nathan William Rodriguez

A thesis submitted to the faculty of
Brigham Young University
in partial fulfillment of the requirements for the degree of

Master of Science

Joshua L. Andersen, Chair
Kenneth A. Christensen
Richard Kent Watt

Department of Chemistry and Biochemistry

Brigham Young University

ABSTRACT

Acylation of Superoxide Dismutase 1 (SOD1) at K122 Alters SOD1 Localization and SOD1-Mediated Inhibition of Mitochondrial Respiration

Nathan William Rodriguez
Department of Chemistry and Biochemistry, BYU
Master of Science

Cu/Zn Superoxide Dismutase (SOD1), is a ubiquitous antioxidant enzyme with several emerging roles outside of its canonical function. SOD1 is also emerging in central roles in cancer and neurodegenerative pathologies. Little is known about SOD1 regulation, particularly at a post-translational level. Post-translational modifications (PTMs) play an important role in enabling proteins to rapidly respond to their environment. Therefore, identifying specific PTMs involved in protein regulation represents a powerful opportunity to interfere with any associated pathologies.

This work employs proteomics to identify mechanisms of post-translation regulation on cell survival signaling proteins. We focused on SOD1, which protects cells from oxidative stress. We found that acylation of K122 on SOD1, while not impacting SOD1 catalytic activity, suppressed the ability of SOD1 to inhibit mitochondrial metabolism at respiratory complex I. We found that deacylase depletion increased K122 acylation on SOD1, which blocked suppression of respiration in a K122-dependent manner. In addition, we found that acyl-mimicking mutations at K122 decreased SOD1 accumulation in mitochondria, initially hinting that SOD1 may inhibit respiration directly within the intermembrane space (IMS). However, surprisingly, we found that forcing the K122 acyl mutants into the mitochondria with an IMS-targeting tag did not recover their ability to suppress respiration. Moreover, we found that suppressing or boosting respiration levels toggled SOD1 in or out of the mitochondria, respectively. These findings place SOD1-mediated inhibition of respiration upstream of its mitochondrial localization. Interestingly, we also found that K122 acyl mutants were sufficient to prevent mitochondrial accumulation of the G93A SOD1 clinical mutant. We observed increased autophagic activity in G93A expressing cells compared to WT or G93A/K122-acyl mimic double mutants, and found that this double mutant was just as prone to aggregate as G93A SOD1—suggesting that SOD1 aggregation is more toxic when in the mitochondria. We observed increased protein turnover rates in cells expressing SOD1 G93A, in support of increased autophagy. Lastly, deletion-rescue experiments show that a respiration-defective mutant of SOD1 is also impaired in its ability to rescue cells from toxicity caused by SOD1 deletion. Together, these data suggest a new interplay between SOD1 acylation, metabolic regulation, SOD1 aggregate toxicity, and SOD1-mediated cell survival.

Keywords: superoxide dismutase, SOD1, mitochondria, SIRT5, respiration, PTM, autophagy

ACKNOWLEDGEMENTS

I thank my wife foremost, for supporting me and encouraging me throughout my time in this degree program. I thank my colleague, Courtney Banks for much appreciated help with experiment planning, data acquisition, and figure preparation. I thank Kyle Gashler for his support and encouragement, as well. I thank my committee chair, Dr. Josh Andersen for high quality mentoring and support with my career goals. I thank Dr. Ken Christensen for his valuable insight and encouragement, as well as for his support with my career goals. I thank Dr. Richard Watt for valuable feedback and constant attentiveness to my career goals. I am very grateful to all the members of the Andersen Lab. This experience would have been nothing without them. I also thank the many other graduate and undergraduate students in the department who were there to share in the good times as well as the bad. I thank the Department of Chemistry and Biochemistry and all the amazing office staff who were always incredibly helpful and kind. What a wonderful group of people.

CONTENTS

LIST OF FIGURES

CHAPTER 1: INTRODUCTION TO SOD1 AND DISEASE

Enzymatic and other functions

Superoxide dismutase 1 (SOD1) is a copper/zinc based metalloprotein whose best characterized function is to scavenge superoxide anion (O_2^-), a type of reactive oxygen species (ROS), and break it down into hydrogen peroxide (H_2O_2) and molecular oxygen (O_2). This antioxidant role for SOD1 is important for cell maintenance, both in terms of health and signaling. At high concentrations, ROS can cause oxidative stress, initiate radical chemistry, and react with DNA, lipids, and proteins (1, 2). Genomic instability caused by oxidative damage contributes to several pathologies, including carcinogenesis, ageing, diabetes, as well as neurological and cardiovascular diseases (2-4). Despite being toxic at high concentrations, at lower to intermediate levels, ROS in general act as a kind of byproduct signaling molecule. For example, as reviewed by Finkel, ROS can regulate growth factor response, and also assist with inflammatory response initiation (5). Therefore, by moderating ROS levels, SOD1 not only abates oxidative stress and cellular damage, but also plays an indirect role in cellular signaling pathways.

The idea of SOD1 as a signaling protein, however, is not novel. Interestingly, although SOD1 is primarily thought of as an antioxidant, in yeast ~1% of SOD1 expressed in cells is sufficient to maintain ROS below cytotoxic levels (6). And given that it is known to localize primarily to the cytosol, but also to the nucleus as well as mitochondria, it is easy to imagine that, in addition to ROS scavenging, SOD1 may have additional functions. For example, Tsang et al. as well as Wood and Thiele have described SOD1 as exerting transcription-regulatory function within the nucleus (7, 8). It has also been shown that SOD1 plays an active role in

copper and zinc buffering (9, 10). Furthermore, another group has proposed that SOD1 may compete with cytochrome c oxidase (CcO) for copper from a common pool within the mitochondrial intermembrane space (11, 12), and therefore SOD1 would indirectly regulate mitochondrial respiration by limiting CcO function in the electron transport chain. Beyond these findings, Reddi and Culotta showed that SOD1 in yeast is important for directly regulating mitochondrial respiration through binding interactions with Wnt signaling proteins (13). Specifically, they showed SOD1 suppresses respiration by binding and stabilizing two casein kinase 1-gamma homologs. Together, these studies strongly suggest a multifaceted role for SOD1 in the cell.

Dysregulation, disease, and autophagy

SOD1 mutations are strongly implicated in the neurodegenerative disease amyotrophic lateral sclerosis (ALS). Specifically, 5–10% of all ALS cases are familial, and SOD1 mutations account for about 20–25% of all familial cases (14-17). There are at least 160 identified SOD1 mutations known to cause ALS (18). The precise mechanisms underlying how these mutations lead to ALS are unclear and heavily debated. In most cases, however, it is accepted that these mutations induce SOD1 to misfold and aggregate, and that these aggregates cause downstream pathological effects (18). Observed phenotypes include mitochondrial metabolism deficiencies, axonal failure, overwhelming of the proteasome, and endoplasmic reticulum stress (18), the outcome of which is often motor neuron cell death.

Extensive work has been done to characterize how SOD1 mutations lead to aggregation and why those aggregates are toxic. Münch and Bertolotti found that many SOD1 mutations may expose or create additional hydrophobic surface area (19). Elam et al. found that SOD1

mutations sometimes interfere with copper and/or zinc loading into SOD1 (20), and Tiwari et al. found that metal-deficient SOD1 is prone to expose hydrophobic faces (21). These hydrophobic faces then favor direct intermolecular interactions with the same face of other mutant SOD1 proteins. Additionally, in 2011, it was shown that these same hydrophobic faces function as nucleation sites for aggregates on the surfaces of lipid membranes (22). Interestingly, Brian Shaw's group found that aspirin-induced hyperacetylation of mutant, aggregate-prone SOD1 increased its net negative surface charge and significantly reduced aggregation, suggesting that net charge may contribute to SOD1's propensity to aggregate (23).

Whatever the mechanism for aggregation, it is clear that SOD1 aggregates play a principle role in mutant SOD1's toxic gain-of-function, although how and why remains unsolved. Many groups agree that the proteotoxic stress caused by overwhelming quantities of SOD1 aggregates lead to mutant SOD1's neurodegenerative effects. Particularly, Pickles et al. posit that aggregation of misfolded SOD1 within the mitochondria is damaging and eventually detrimental to neurons (24). As one possible explanation for the proteotoxicity, Zhang et al. showed that SOD1 aggregation in ALS mice leads to a stalled cell recycling process known as autophagy (25), which will be further discussed in chapter 3.

SOD1 is also reportedly overexpressed in several cancers, including lung adenocarcinoma (26), non-small-cell lung cancer (27), and 70% of primary breast cancers (28). Cancer cells often experience ischemia and must adapt to a hypoxic, low-glucose environment, which results over time in higher ROS concentrations (29, 30). In the context of cancer, increased SOD1 may benefit cells by neutralizing excess ROS and thereby increasing their rate of survival. Interestingly, it may also be possible that SOD1's respiration-suppressing capacity

further enable cell survival by promoting alternate metabolic pathways, such as the Warburg Effect, which is characterized by reduced mitochondrial respiration.

These functions of SOD1 suggest a complex mode of pathogenicity and more importantly, regulation. Yet how SOD1 is regulated remains unknown, particularly on a post translational level. Elucidating these regulatory mechanisms could allow for manipulation of SOD1 prior to or during disease progression.

SOD1 Regulation

In 2009, proteomics work done by Choudhary, et al. identified K122 of SOD1 as an acetylation target (31). K122 is an amino acid residue that lies within a highly conserved and functionally critical domain of SOD1 known as the electrostatic loop. The amino acid residues in this loop help direct superoxide anions to the active site of SOD1 (32). One of these residues is a histidine responsible for binding copper, which is necessary for SOD1 to scavenge ROS (33). Previous studies show that some mutations within this loop, or of residues that stabilize this loop, compromise SOD1 activity (34). This evidence indicates the importance of residues within the electrostatic loop region, including K122.

In 2011, Andersen, et al. identified the same SOD1 K122 as an acetylation target in the context of tumor like oxidative stress (35), suggesting that this acyl modification may alter SOD1 function in response to glucose and oxygen limited conditions. In 2013, Park, et al. identified this same residue as a target for succinylation in response to knock out of SIRT5, a well characterized desuccinylase (36). Later that year, Lin, et al. correlated this post translational modification (PTM) with reduced antioxidant activity (37). These PTMs occurred naturally, and in response to different physiological conditions, strongly suggesting that SOD1 may exhibit a

post-translational mode of regulation, possibly at K122. Based on these findings and work in our lab, we hypothesized that acetylation and succinylation (acylation) of SOD1 K122 modulate SOD1 antioxidant and respiratory function to help cells adapt to adverse conditions and nutrient stress.

Here, we study the previous findings on K122 acetylation and succinylation, and take them further by putting them in context of SOD1 regulation. We examine the effect of SOD1 K122 acylation on catalytic activity, and its role in mitochondrial metabolism and respiration. We validate the role of SIRT5 in governing SOD1 K122 desuccinylation and look at the effects of SIRT5 depletion on SOD1-mediated suppression of respiration. We also examine the relationship between mitochondrial respiration, SOD1 K122 acylation, and SOD1 localization and where SOD1 exerts its regulatory effect on respiration. Our findings offer novel understanding of SOD1's mode of regulation as well as valuable insight into SOD1's role in promoting cell growth and survival. Our data suggest a feed-forward loop wherein SIRT5 deacylates K122, after which SOD1 represses mitochondrial respiration, leading to SOD1 mitochondrial localization. We postulate that this mechanism may provide pro-survival benefits to cells. Further work is needed to determine if these acylations interfere with interactions between SOD1 and known regulators of respiration.

CHAPTER 2: ACYLATION OF SUPEROXIDE DISMUTASE 1 (SOD1) AT K122 GOVERNS SOD1-MEDIATED INHIBITION OF MITOCHONDRIAL RESPIRATION

INTRODUCTION

The regulation of cell signaling events through protein post-translational modifications (PTMs), including phosphorylation, acylation, glycosylation and ubiquitination, provides a means for cells to respond rapidly to environmental cues. Defects in the pathways that control PTMs underlie many human diseases and typically represent a fundamental breakdown in communication between the cell and its environment. Mass spectrometry-based approaches have dramatically expanded our view of PTMs, both in terms of PTM variety and proteome coverage. Over 200 different PTMs have been described (uniprot.org) and many, including phosphorylation and ubiquitination, regulate essentially every known biological process in the cell. With this understanding of PTM breadth, the challenge is to now 'zoom in' to understand the functional consequences of specific PTMs. Thus, our goal is to understand how PTMs affect protein function, with particular focus on cell survival signaling nodes and pathways.

Here we used an affinity purification approach, coupled with liquid chromatography tandem mass spectrometry (LC-MS/MS), to identify PTMs in primary untreated mouse tissues. Using a recently developed PTM analysis tool (SAPH-ire) to prioritize our functional studies, we evaluated PTMs from our experiment against all other experimentally observed PTMs curated for the Cu/Zn Superoxide Dismutase (SOD) domain family (38, 39). This analysis highlighted an acyl-modified lysine on SOD1, which we focused on in this study. SOD1 is a well conserved metalloenzyme best known for its catalytic role in disproportionation of superoxide radicals (O_2^-) into molecular oxygen (O_2) and hydrogen peroxide (H_2O_2) (9, 40-47). Its expression is primarily

cytosolic, although a fraction of SOD1 exists in the mitochondrial intermembrane space (IMS). Studies spanning multiple model organisms and cell lines have underscored the importance of SOD1 in oxidative stress protection (reviewed in (48, 49)). Accordingly, SOD1 is overexpressed in a variety of cancers and SOD1 deletion in mice results in a higher incidence of liver cancer (43). Additionally, mutations in SOD1 that increase its propensity to aggregate cause toxicity in motor neurons, resulting in a familial form of amyotrophic lateral sclerosis (ALS) (reviewed in (49)).

Several lines of evidence suggest that SOD1 biology may be more complex than initially thought. While SOD1 deletion is toxic in cultured cells due to an accumulation of oxidative damage (50, 51), titration of SOD1 expression against a SOD1 null background in yeast revealed that only a small fraction, representing about 1% of total SOD1, is required for protection against oxidative stress (6). This suggests that SOD1 may have additional functions beyond its traditional role in reactive oxygen species (ROS) scavenging. Indeed, studies suggest that SOD1 has roles in zinc and copper buffering (9, 10) and in regulating gene transcription (7, 8). In addition, a recent study by Reddi and Culotta found that yeast SOD1 suppressed mitochondrial respiration (13). However, despite this emerging complexity in SOD1 biology and clear roles for SOD1 in human disease, we have a limited understanding of SOD1 regulation at a post-translational level.

Here we uncover a novel regulatory mechanism by which a Sirtuin-governed acylation within the electrostatic loop of SOD1, at K122, suppresses SOD1-mediated inhibition of mitochondrial metabolism in mammalian cells. This observation provided genetic tools to help understand the relationship between SOD1 mitochondrial localization and metabolic regulation as well as the potential contribution of this SOD1 metabolic function to its role in promoting cell survival. Our data suggest a model in which Sirtuin-mediated deacylation of SOD1 promotes its

inhibition of respiration, which in turn, elevates levels of mitochondrial SOD1 and contributes to SOD1's pro-survival function.

RESULTS

With the goal of identifying PTMs on cell survival signaling nodes, we used, as a starting point, several PTM-specific antibody resins to compare *in vivo* PTMs across multiple mouse tissues (brain, liver, and embryo homogenates). The experimental layout is shown in Figure 1A and included several phospho-motif, ubiquitin and acetyl-lysine affinity resins. A complete set of database search results from this experiment are publicly available as a Scaffold file (Proteome Software Inc.) at https://discovery.genome.duke.edu/express/resources/3023/3023_PTMScanAll_withTiO2.sf3. In an effort to zoom in on PTMs on cell survival signaling nodes, we applied gene ontology analysis, as well as manual sorting by protein function. Two proteins of interest, 14-3-3ζ and SOD1, are shown in Figure 1B. 14-3-3ζ is a phospho-serine/threonine binding protein that is overexpressed in a variety of cancers and promotes cell survival by directly modulating a network of phospho-proteins. In combining our PTM data sets, we identified PTMs on 14-3-3ζ of unknown function, including phospho-Y149, Ub-K139, in addition to well-described PTMs, such as Ac-K49 (31, 35, 52). In particular, acetylation of K49 is known to disrupt 14-3-3ζ interactions and our previous work identified HDAC6 as the K49-targeted KDAC (52).

SAPH-ire identifies PTMs with high function potential in the SOD domain family. Our attention was also drawn to SOD1, which acts as one of the main modes of defense against oxidative stress by catalyzing the disproportionation of superoxide radicals (O_2^-) to molecular oxygen (O_2) and hydrogen peroxide (H_2O_2). Figure 1B lower panel shows the crystal structure of

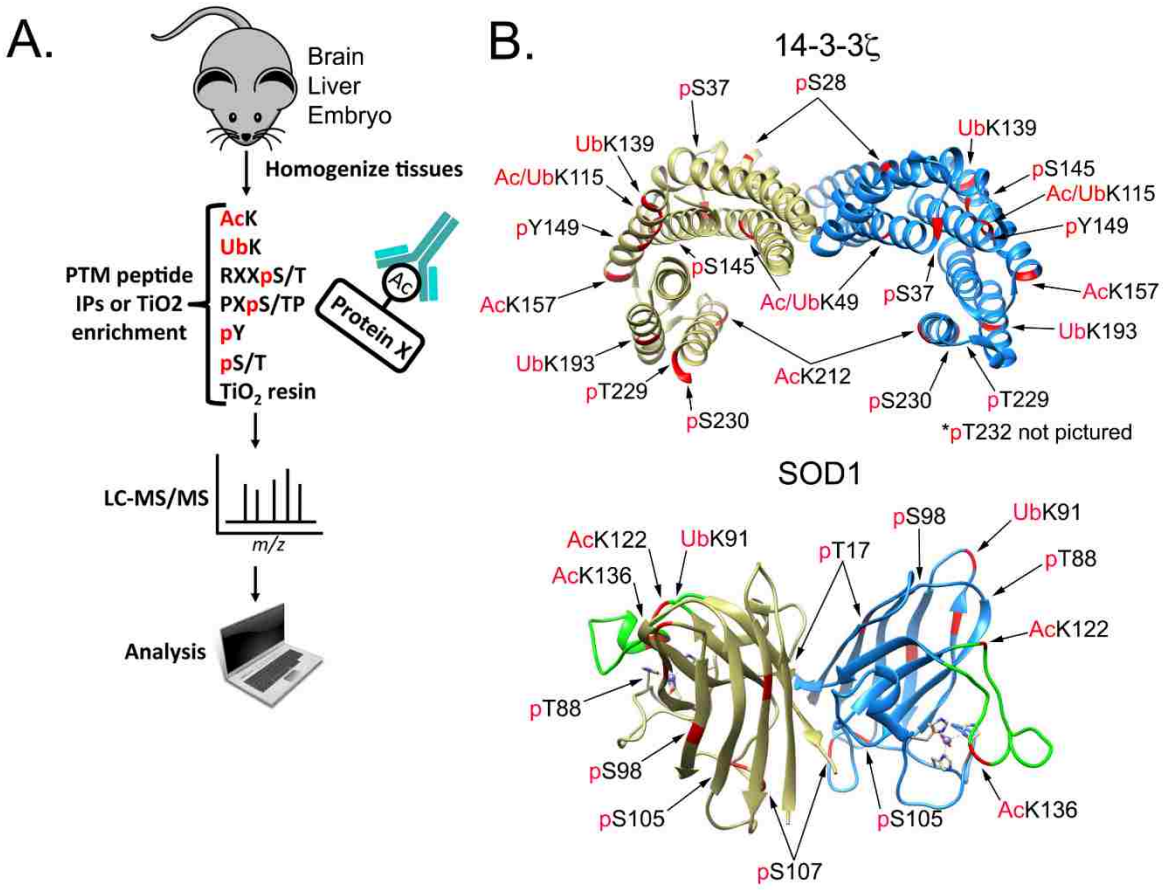

Figure 1. Identification of PTMs on 14-3-3ζ and SOD1. **(A)** Brain, liver, and whole embryo mouse tissues were homogenized and digested with trypsin. Peptides were subject to affinity purification by the indicated antibody resin. Peptides were eluted and analyzed by LC/MS/MS. Proteomics data were analyzed with Scaffold software. **(B)** Crystal structures of human 14-3-3ζ (PDB: 4IHL) and mouse SOD1 (PDB: 3GTT) with PTMs identified in the proteomics data.

the SOD1 dimer and PTMs identified from our proteomics data. In an effort to prioritize PTMs on SOD1, we utilized SAPH-ire FPx, a machine-learning-based PTM "hotspot" finder that examines experimentally-identified PTMs and prioritizes the PTMs for likelihood of biological function based on a number of parameters as previously described (38, 39, 53). Using human SOD1 (UniProt ID: P00441) as an anchor, PTMs were evaluated in the context of the entire eukaryotic SOD domain family (InterPro ID: IPR001424). Interestingly, PTMs localized in the region

between S98 and K128 exhibited the highest SAPH-ire FPx scores across the entire domain (Figure 2A). In fact, the top seven PTM sites with the highest FPx score were all within this region (Figure 2B-D). We became interested in an acylated lysine (K122) that was found not only in our mouse proteomics data set but was also identified by SAPH-ire in the region with the highest FPx scores and was one of the top two highest ranking modified lysine hotspots in the SOD domain family (Figure 2A-D). In comparing the two acyl-lysines (K122 and K128) within the top SAPH-ire cluster, K122 had the highest number (eight) of co-aligned PTMs in the family (indicated by circle size) and also the second highest number (five) of independent MS-based observations (indicated by circle color, Figure 2A-C), suggesting that K122 may be an important regulatory site. K122 sits within the electrostatic loop (Figure 2E), which has nearby residues (H120 and D124) important for binding zinc and copper (54). K122 is conserved from human to bird (Figure 2F), and has been identified in previous studies, among other acyl-lysines, as acetylated and succinylated (31, 37, 55-57) (Figure 2G). A study by Lin et al. found that SIRT5 desuccinylates K122 and it was proposed to affect SOD1 antioxidant activity (37). In addition, a recent study using a site-specific antibody demonstrated that K122 is acetylated on endogenous SOD1 in multiple cell types throughout the murine nervous system (58), although the impact of the acetyl modification on SOD1 function was not demonstrated. With this background, we investigated the functional impact of K122 acylation on SOD1.

Acyl-mimicking mutations at K122 have no effect on SOD1 dimerization or ROS scavenging activity. To examine the effect of acylation at K122 on various SOD1 functions, we generated acetyl-mimicking K122Q and succinyl-mimicking K122E mutations. Although there are structural differences between glutamine/glutamate and N^{ε}-acyl-lysine, these mutations mimic

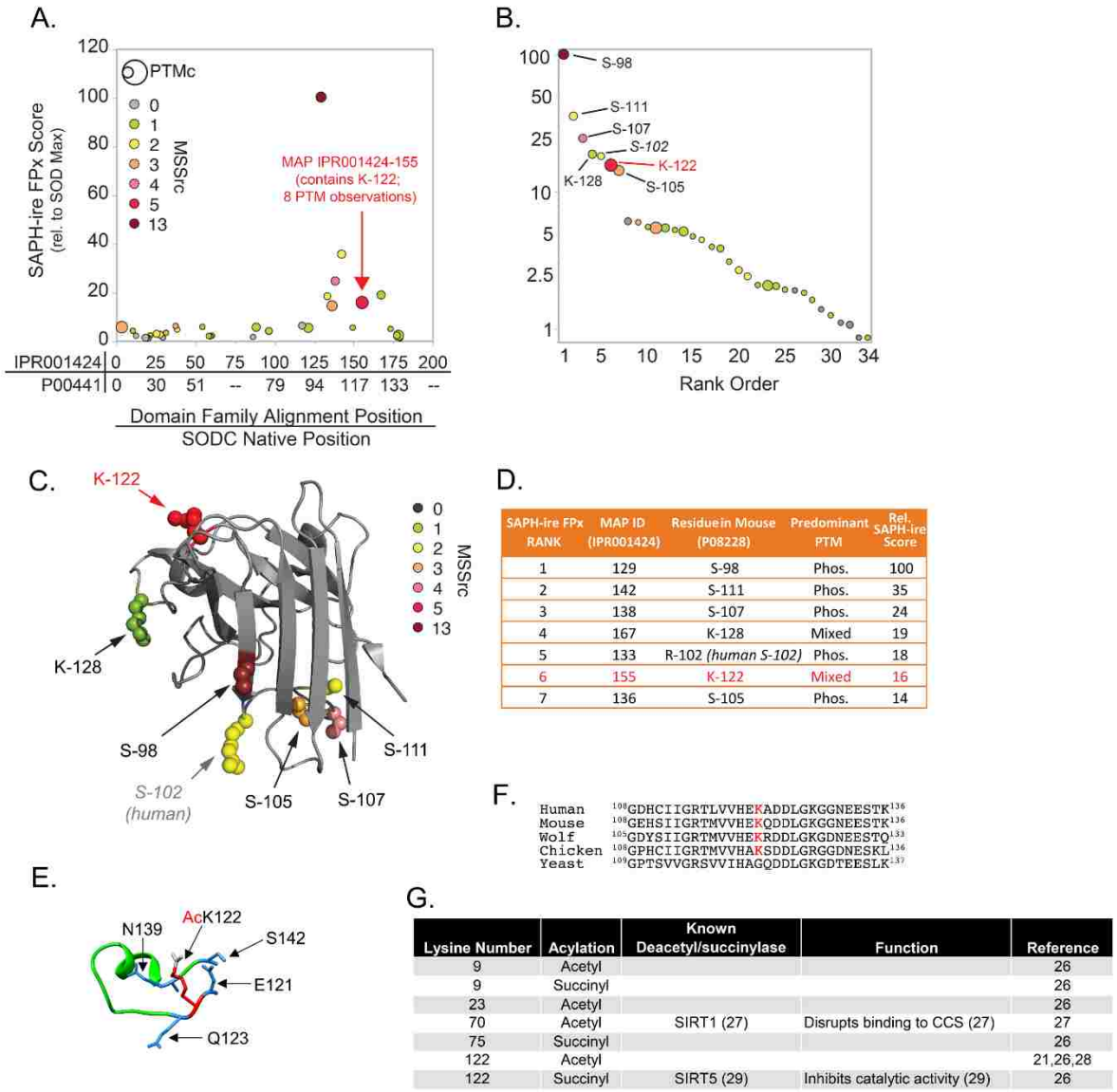

SAPH-ire FPx RANK	MAP ID (IPR001424)	Residue in Mouse (P08228)	Predominant PTM	Rel. SAPH-ire Score
1	129	S-98	Phos.	100
2	142	S-111	Phos.	35
3	138	S-107	Phos.	24
4	167	K-128	Mixed	19
5	133	R-102 *(human S-102)*	Phos.	18
6	155	K-122	Mixed	16
7	136	S-105	Phos.	14

Lysine Number	Acylation	Known Deacetyl/succinylase	Function	Reference
9	Acetyl			26
9	Succinyl			26
23	Acetyl			26
70	Acetyl	SIRT1 (27)	Disrupts binding to CCS (27)	27
75	Succinyl			26
122	Acetyl			21,26,28
122	Succinyl	SIRT5 (29)	Inhibits catalytic activity (29)	26

Figure 2. SAPH-ire identifies PTMs with high function potential in the SOD domain family. (A) Plot of SAPH-ire function potential score for 34 modified alignment positions (MAPs) along the length of the SOD domain family. Domain family alignment position and corresponding native position of human SOD1 are plotted on the x-axis for reference (from N- to C-terminal). The number of distinct PTMs observed within a MAP (PTM count; PTMc) is represented by circle size. The number of independent literature sources documenting observation of PTMs in each MAP (Mass Spec Source Count; MSSrc) is indicated by circle color. **(B)** Rank ordered plot of SAPH-ire function potential scores for the 34 SOD domain family MAPs. Residue positions correspond to mouse SOD1 residues found in each of the top 7 domain family MAPs. **(C)** Projection of the top 7 MAPs onto the crystal structure of mouse SOD1 (UniProt ID: P08228) (PDB: 3GTT, Chain A). **(D)** Table summarizing the identities and predominant PTMs observed

for each of the top 7 SOD MAPs. **(E)** Zoomed in crystal structure of the mouse SOD1 (PDB: 3GTT) electrostatic loop featuring K122 (red) modified with an acetyl group (grey) and surrounding amino acids (blue). **(F)** Sequence alignment of human, mouse, wolf, chicken, and yeast SOD1 with K122 highlighted in red. **(G)** Table indicating all known lysine acetyl or succinyl modifications of human SOD1, known deacetyl/succinylases, and phenotype of the modifications.

the change in charge associated with the acyl modifications. One limitation of this approach is that the mutations abrogate any other lysine modification (e.g., ubiquitin) that may occur at the site, thus comparison with the K-to-R control (mimics a non-acylated lysine, but also abrogates other lysine PTMs) is critical. To determine whether the acyl-mimicking mutants could dimerize with WT SOD1, we overexpressed Flag-tagged WT SOD1 together with either HA-tagged WT SOD1 or HA-tagged mutant SOD1 in HEK-293 cells and saw no difference in dimerization between WT and acyl-mimicking SOD1 mutants (Figure 3A). We also saw no difference in the binding of these SOD1 mutants to the copper chaperone for superoxide dismutase (CCS; Figure 3B), which promotes the final stage of SOD1 folding and maturation. Furthermore, in contrast to the study by Lin et al. (37), we found no difference in ROS scavenging between WT and the acyl-mimicking SOD1 mutants. This was verified in multiple ROS scavenging assays with purified SOD1, a nitrotetrazolium blue gel assay, and included the ROS scavenging-impaired SOD1 point mutant G85R, as a positive control (Figures 3C and 3D).

K122 acyl-mimics inhibit SOD1-mediated control of mitochondrial respiration. Although SOD1 is commonly thought of as an antioxidant, only 1% of SOD1 expressed in cells is necessary to keep ROS below cytotoxic levels (6). The rationale for such high levels of SOD1 has led others to propose that it may have important functions beyond disproportionation of oxygen radicals (13). Previous studies have suggested SOD1 has roles in cellular zinc (10) and copper

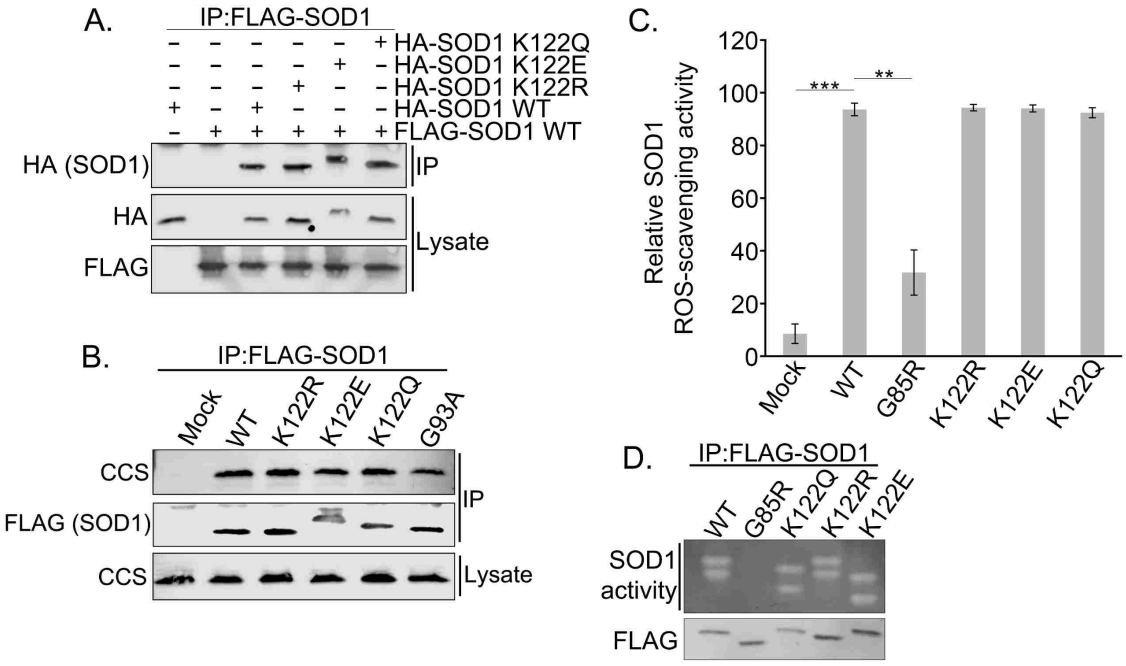

Figure 3. Acyl-mimic mutations at K122 of SOD1 do not affect canonical SOD1 ROS scavenging activity. (A) HEK 293 cells were co-transfected with Flag-tagged WT SOD1and HA-tagged WT, K122R, K122E, or K122Q SOD1 expression plasmids. Flag-WT SOD1 was immunoprecipitated with Flag agarose resin and run through SDS-PAGE before being immunoblotted for HA-tagged binding partners. **(B)** HEK 293 cells were transfected with Flag-tagged WT, K122R, K122E, K122Q, or G93A SOD1 expression plasmids. Flag-tagged SOD1 was immunoprecipitated with Flag agarose resin and run through SDS-PAGE before being immunoblotted for the CCS binding partner. **(C)** HEK 293 cells were transfected with Flag-tagged WT, G85R, K122R, K122E, or K122Q SOD1. SOD1 was immunoprecipitated with Flag agarose resin and then competitively eluted with Flag peptide. The eluted SOD1 activity was then measured calorimetrically. (n=3; **p<0.01, ***p<0.001; error bars are represented by +/- SEM) **(D)** Samples were prepared as in (C) and the eluted SOD1 was resolved through Native-PAGE and SOD1 activity was assayed within the gel. White bands indicate active SOD1.

buffering (9), and as a nuclear transcription factor (7, 8). In addition, a more recent study by Reddi et al. demonstrated a novel function of yeast SOD1 in suppressing mitochondrial respiration through modulation of casein kinase signaling (13). Given that lysine acylation is linked to metabolism (31, 59, 60), we decided to test the potential link between the K122 PTM and SOD1

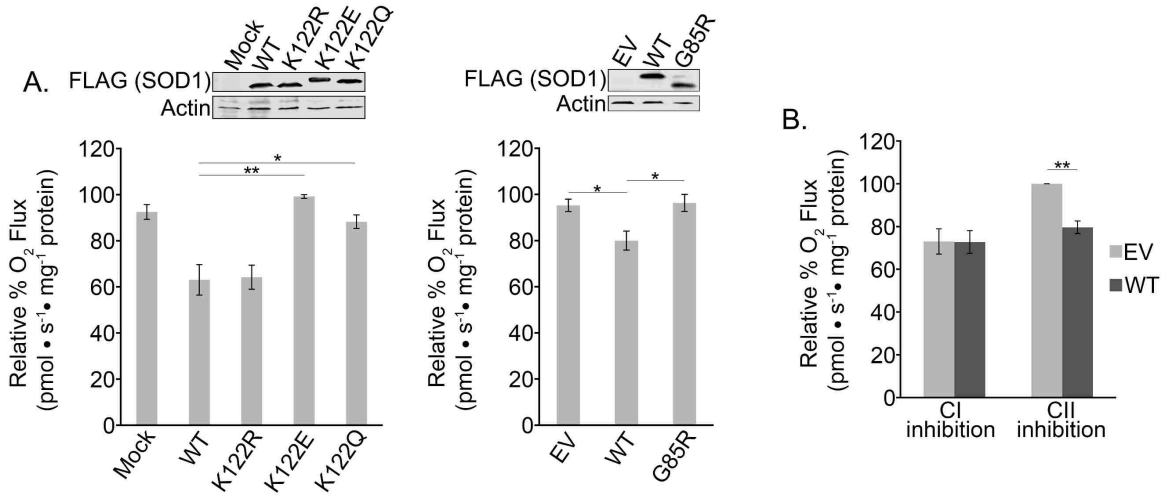

Figure 4. Acyl-K122 mimics of SOD1 inhibit SOD1-mediated suppression of mitochondrial respiration. (A) Left: HEK 293 cells were transfected with Flag-tagged WT, K122R, K122E, or K122Q SOD1 expression plasmids and oxygen flux was measured with an Oroboros O2K respirometer. Cell lysates were separated by SDS-PAGE and immunoblotted for Flag-SOD1. (n=4; *p<0.05, **p<0.01; error bars are represented by +/- SEM) Right: HEK 293 cells were transfected with an empty vector or Flag-tagged WT, or G85R SOD1 expression plasmids and assayed as in the left panel. (n=3; *p<0.05; error bars are represented by +/- SEM) **(B)** HEK 293 cells were transfected with an empty vector or Flag-tagged WT SOD1 expression vector. Oxygen rates were measured with an Oroboros O2K respirometer after CI inhibition with rotenone (2 mM) or CII inhibition with malonate (2.5 mM). (n=3 technical replicates; **p<0.01; error bars are represented by +/- SEM)

anti-respiratory activity. To first test whether mammalian SOD1 suppresses respiration like its yeast counterpart, we expressed WT human SOD1 in HEK-293 cells and saw a marked decrease in mitochondrial oxygen flux, suggesting conservation of this SOD1 metabolic function from yeast to humans (Figure 4A). Importantly, in comparing this effect on respiration across the panel of acyl-mimicking SOD1 mutants, we found that the acetyl (K122Q)- and succinyl (K122E)-mimicking mutants completely lost their ability to suppress respiration. Like yeast SOD1, the inhibitory effect of mammalian SOD1 on respiration required its enzymatic activity, as the G85R mutant, which shows ~70% reduced ROS scavenging activity compared to WT (Figure 3C), failed

to inhibit respiration like WT SOD1 (13). As an additional control, the K122R mutant was fully active in suppressing respiration, suggesting that the K122Q and K122E phenotypes were not simply due to mutation of the lysine, which could block other lysine PTMs, such as sumoylation or ubiquitination (Figure 4A).

To determine which ETC subunit complex was affected by SOD1, we treated the SOD1-expressing cells with inhibitors of complex I and II. While complex II does not transport protons across the intermembrane space like complex I, the two complexes work in parallel to transfer electrons to a pool of ubiquinone. Electrons from ubiquinone are then transferred step-wise to complex IV where molecular oxygen is reduced to water. Because complex I and complex II work in parallel to transfer electrons, each can be inhibited separately and electrons can still be transferred through the uninhibited complex. When we inhibited complex II with malonate, SOD1 was still able to suppress respiration. However, when complex I was inhibited with rotenone, SOD1 had no additional effect on respiration (Figure 4B), suggesting that SOD1 is inhibiting the ETC at complex I.

SOD1-mediated inhibition of respiration can be modulated via SIRT5. Lysine acylation is regulated by the activity of lysine deacylases (KDACs), which include the histone deacetylase (HDACs) and Sirtuin families. Unlike many KDACs which prefer acetyl-lysine as their substrate, SIRT5 shows preference toward the longer chain length acylations of succinylation and malonylation (61). It was previously shown that SIRT5 is the desuccinylase for K122 (37) and, while SIRT5 is traditionally thought of as a mitochondrial Sirtuin, recent studies have described SIRT5's presence in the cytosol as well (62-64). We validated the role of SIRT5 in desuccinylating K122 by developing an antibody specific for succinylated K122 (Su-K122, Figure 5A). To confirm that succinylation occurs on endogenous SOD1, we depleted cells of SIRT5 and

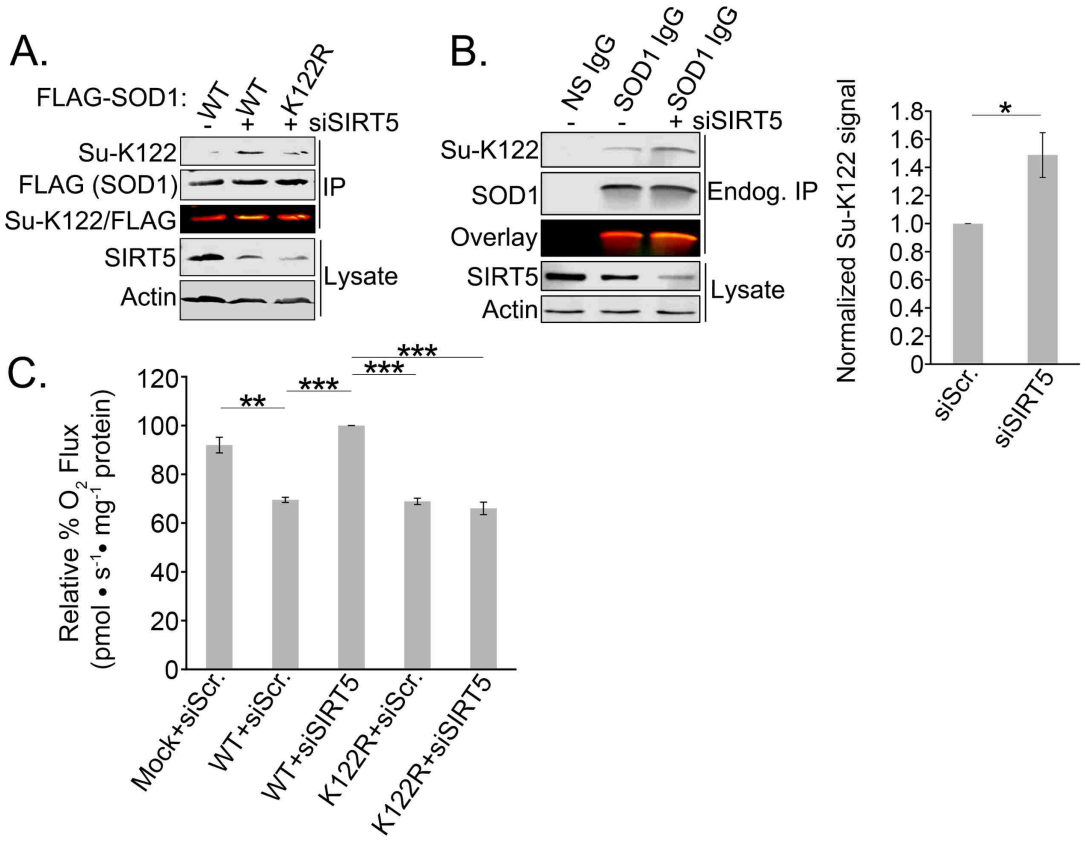

Figure 5. Development of an antibody specific to acylated K122 of SOD1; SIRT5 inhibition results in succinylation of endogenous SOD1. (A) Flag-tagged WT or K122R SOD1 was overexpressed in HEK 293 cells with or without SIRT5 knocked down by siRNA. Flag SOD1 was immunoprecipitated with Flag agarose resin, run through SDS-PAGE and immunoblotted for succinyl-K122 (Su-K122) and total (Flag) SOD1. **(B)** Endogenous SOD1 was immunoprecipitated from HEK 293 cells with or without SIRT5 knocked down via siRNA. The immunoprecipitated SOD1 was then run through SDS-PAGE and immunoblotted with Su-K122 antibody. (n=3; *p<0.05; error bars are represented by +/- SEM) **(C)** Flag-tagged WT or K122R SOD1 was overexpressed in HEK 293 cells with or without SIRT5 knocked down by siRNA. Oxygen rates were measured with an Oroboros O2K respirometer. (n=3; **p<0.01, ***p<0.001; error bars are represented by +/- SEM)

immunoprecipitated SOD1. Figure 5B shows the increase in endogenous SOD1 succinylation at K122 in SIRT5-depleted cells. Although acetylation of K122 clearly occurs on endogenous SOD1 ((31, 55, 57, 58), proteomics data), our attempts to generate site-specific acetyl-K122 antibodies

resulted in limited success—antibodies showed marginal specificity to the acetylation. This complication, combined with the fact that K122E showed a slightly more robust effect in inhibiting SOD1's anti-respiration function, led us to focus primarily on K122 succinylation.

To determine whether we could block SOD1's anti-respiratory activity by modulating the endogenous deacylation machinery, we depleted SIRT5 in cells expressing WT or the non-succinylatable K122R SOD1 and measured respiration. Remarkably, we found that SIRT5 depletion recovered normal respiration levels in cells expressing WT SOD1 and the recovery was overridden by the K122R mutant which cannot be acylated (Figure 5C). This suggests that SIRT5 modulates metabolism via desuccinylation of SOD1 at K122.

SOD1-mediated suppression of respiration is upstream of its mitochondrial localization. SOD1 is known to reside in the cytosol, IMS of the mitochondria, and the nucleus (28). Our respiration data made us question whether the anti-respiratory effect of SOD1 is exerted locally within the IMS. If so, we would predict that acylation of K122 blocks SOD1 mitochondrial localization. As shown in Figure 6A, we found decreased levels of the acyl-mimicking SOD1 mutants in the mitochondrial fraction. We included the ALS-linked G93A SOD1 mutant as a positive control because it is known to accumulate in the IMS (Figure 6A, lane 2) (65). Shaw and colleagues recently showed that neutralization of positively charged lysines by aspirin-induced lysine acetylation on SOD1 inhibited its propensity to aggregate (23). However, the acyl-mimicking mutant, in the context of the ALS-linked G93A mutation, did not decrease SOD1 accumulation (Figure 6B). Together, these data suggest that acylation at K122 inhibits mitochondrial accumulation of SOD1 and, while only correlative, they raise the possibility that the mitochondrial pool of SOD1 may directly inhibit respiration in the IMS.

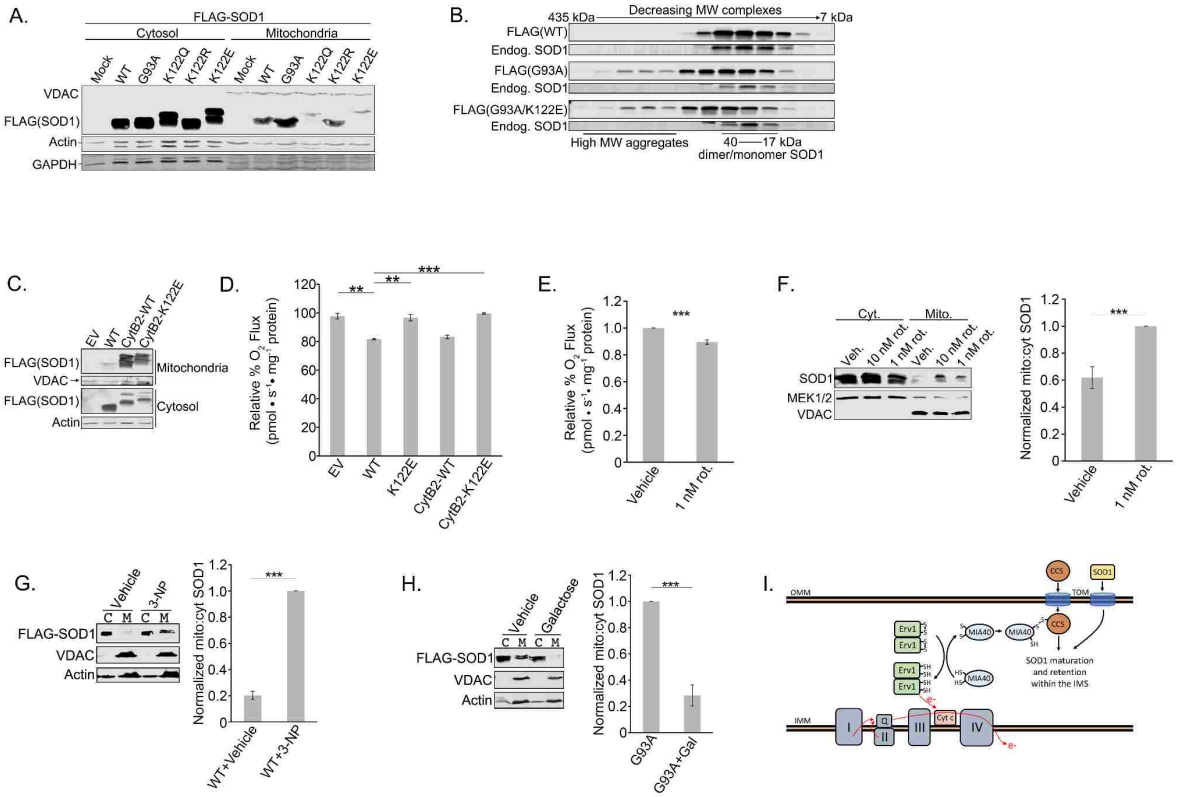

Figure 6. SOD1-mediated suppression of respiration is upstream of its mitochondrial localization. (A) HEK 293 cells were transfected with Flag-tagged WT, G93A, K122Q, K122R, or K122E SOD1. The cells were lysed and mitochondria were fractionated from the cytosol. The two fractions were run through SDS-PAGE and immunoblotted for Flag-SOD1 present in the mitochondria vs. the cytosol. **(B)** Flag-tagged WT, G93A, or G93A/K122E SOD1 was induced with tetracycline for 48 hours in T-REx 293 cells. The cells were lysed and the lysates were then loaded onto a Superdex 200 10/300 GL Size exclusion column and eluted in fractions. The fractions were run through SDS-PAGE and immunoblotted for Flag-SOD1 and endogenous SOD1. **(C)** Flag-tagged WT, CytB2-WT, or CytB2-K122E SOD1 was overexpressed in HEK 293 cells. The cells were lysed and mitochondria were fractionated from the cytosol. The two fractions were run through SDS-PAGE and immunoblotted for Flag-SOD1 present in the mitochondria vs. the cytosol. **(D)** Flag-tagged WT, K122E, CytB2-WT, or CytB2-K122E SOD1 was overexpressed in HEK 293 cells. Oxygen rates were measured with an Oroboros O2K respirometer. (n=3; **p<0.01, ***p<0.001; error bars are represented by +/- SEM) **(E)** 1 nM rotenone or vehicle were added to HEK 293 cells 30 minutes prior to measuring oxygen consumption rates with an Oroboros O2K respirometer. (n=4; ***p<0.001; error bars are represented by +/- SEM) **(F)** 1 or 10 nM rotenone or vehicle were added to HEK 293 cells 30 minutes prior to lysing the cells and

fractionating the mitochondria from the cytosol as in (A). The fractions were immunoblotted for the presence of endogenous SOD1 in the mitochondria and cytosol. In each replicate, SOD1 levels were normalized to mitochondrial and cytosolic loading controls and then normalized to the ratio of mitochondrial SOD1 in the 1 nM rotenone treated sample. (n=6, ***p<0.001; error bars are represented by +/- SEM) **(G)** Flag-tagged WT-SOD1 was overexpressed in HEK 293 cells. 1 mM 3-nitropropionic acid (3-NP) was added for 16-18 hours before the cells were lysed and mitochondria were fractionated from the cytosol. The two fractions were run through SDS-PAGE and immunoblotted for Flag-SOD1 present in the mitochondria vs. the cytosol. In each replicate, Flag-SOD1 levels were normalized to mitochondrial and cytosolic loading controls and then normalized to the ratio of mitochondrial Flag-SOD1 in the 3-NP treated sample. (n=3; ***p<0.001; error bars are represented by +/- SEM) **(H)** Flag-tagged G93A-SOD1 was overexpressed in HEK 293 cells. 25 mM galactose in low glucose (2 mM) media was added 24 hours before the cells were lysed and assayed as in (G). In each replicate, Flag-SOD1 levels were normalized to mitochondrial and cytosolic loading controls and then normalized to the ratio of mitochondrial Flag-SOD1 in the untreated sample. (n=3; ***p<0.001; error bars are represented by +/- SEM) **(I)** An Erv1/MIA40 disulfide relay promotes the IMS import of CCS, which in turn promotes the IMS retention of SOD1. The disulfide relay is reset when oxidized cytochrome c accepts an electron from Erv1 (model adapted from Kawamata and Manfredi (67)).

Based on these data, our initial hypothesis was that acylation of K122 prevented SOD1 mitochondrial localization and thus blocked SOD1-mediated suppression of respiration. To test this further, we used an approach in which SOD1 is appended, in frame, to the mitochondrial import signal of *Saccharomyces cerevisiae* cytochrome b2 (CytB2) (66). Our prediction was two-fold: First, that pushing WT SOD1 into the IMS would enhance SOD1-mediated suppression of respiration; and second, that forcing the K122E SOD1 mutant into the mitochondria would rescue its ability to suppress respiration. Figure 6C shows validation that the IMS targeting tag resulted in robust accumulation of WT and K122E SOD1 in the mitochondrial fractions. However, to our surprise, the mitochondrial localization of SOD1 did not enhance its ability to suppress respiration (Figure 6D), nor did it recover the ability of the K122E mutant to suppress respiration. This suggests that SOD1's suppression of respiration is independent of its mitochondrial

localization, which agrees with data from yeast in which the respiration-suppressing signal from SOD1 originates in the cytosol (13).

An alternative explanation for the relationship between K122 acylation and SOD1 mitochondrial localization is that SOD1's effect on respiration is upstream of its mitochondrial localization. Indeed, there is evidence that the disulfide relay system that imports SOD1 into the IMS is dependent on electron flux through cytochrome c reductase (complex III) of the ETC (68) (69). Based on this model, up- or down-regulation of respiratory activity would cause a corresponding decrease or increase in SOD1 mitochondrial localization. To test this, we first identified a dose of rotenone, a complex I inhibitor, at 1 nM that produced a 10-15% reduction in overall oxygen consumption (Figure 6E), similar to what we had observed with WT SOD1 in our previous experiments. In support of the idea that inhibition of respiration drives mitochondrial uptake of SOD1, treatment of cells with 1 nM rotenone for 30 minutes significantly increased the accumulation of endogenous SOD1 in the mitochondrial pellet (Figure 6F). Additionally, treatment of cells with 3-nitropropionic acid (3-NP), a complex II inhibitor, also triggered an increase in mitochondrial SOD1 (Figure 6G). Conversely, boosting ETC activity by culturing cells in galactose nearly eliminated the IMS-localized G93A mutant SOD1 from the IMS (Figure 6H). These results suggest that cellular respiration levels modulate SOD1 mitochondrial uptake, such that inhibition or stimulation of respiration can toggle SOD1 mitochondrial accumulation up or down, respectively (model in Figure 6I). Furthermore, this suggests a potential feedback loop between SOD1 acylation, inhibition of respiration and SOD1 mitochondrial import (see discussion).

The SOD1 K122E acyl mimic is impaired in its ability to rescue the lethality of SOD1 deletion and reduce mitochondrial ROS levels. While SOD1's vital role in direct

disproportionation of cytosolic ROS is well established, our observation that SOD1 suppresses respiration at complex I and the link between respiration and SOD1 mitochondrial import may indicate an added dimension to SOD1's role as an antioxidant. This is based on the decades-old observation that the ETC is a source of ROS (70, 71) and the possible role of the mitochondrial pool of SOD1 in scavenging ROS directly within the IMS (72, 73). The K122E mutant provided, to our knowledge, the first tool to address this question genetically because it inhibits SOD1's anti-respiratory function while maintaining SOD1 enzymatic ROS scavenging activity. We took advantage of an HCT-116 cell T-REx-based 'flip-in' system wherein a gene of interest can be stably recombined with a specific locus under the control of a doxycycline (dox)-inducible promoter. This provides the advantage of controlling for copy number, which allows for a more fair comparison between different derived lines. After generating a panel of stable doxycycline-inducible SOD1 variants with silent mutations at PAM sites, we used CRISPR/Cas9 to delete endogenous genomic SOD1 from each of the lines. Figure 7A shows that the inducible system gives near-endogenous levels of WT and K122E SOD1 expression and is completely refractory to the endogenous SOD1-targeted sgRNA. Of note, we had difficulty immunoblotting for G85R after deletion of SOD1 due to the inability of G85R to rescue cells from the acute toxicity of SOD1 KO.

Previous studies have shown that SOD1 deletion in eukaryotes results in cell death as a result of ROS accumulation (50, 51). Consistent with this observation, the SOD1 KO lines showed a dramatic loss of cell growth as measured by an Incucyte live cell analysis system (Figure 7B—upper panel shows basal growth rates without dox treatment) and infrared scanning of Giemsa-stained cultures after cell dilution and growth over a time course (Figure 7C). The loss of growth caused by SOD1 KO was completely reversed in these cells by reconstituting WT SOD1 expression from the dox-inducible locus, indicating that growth defects were not due to off-target

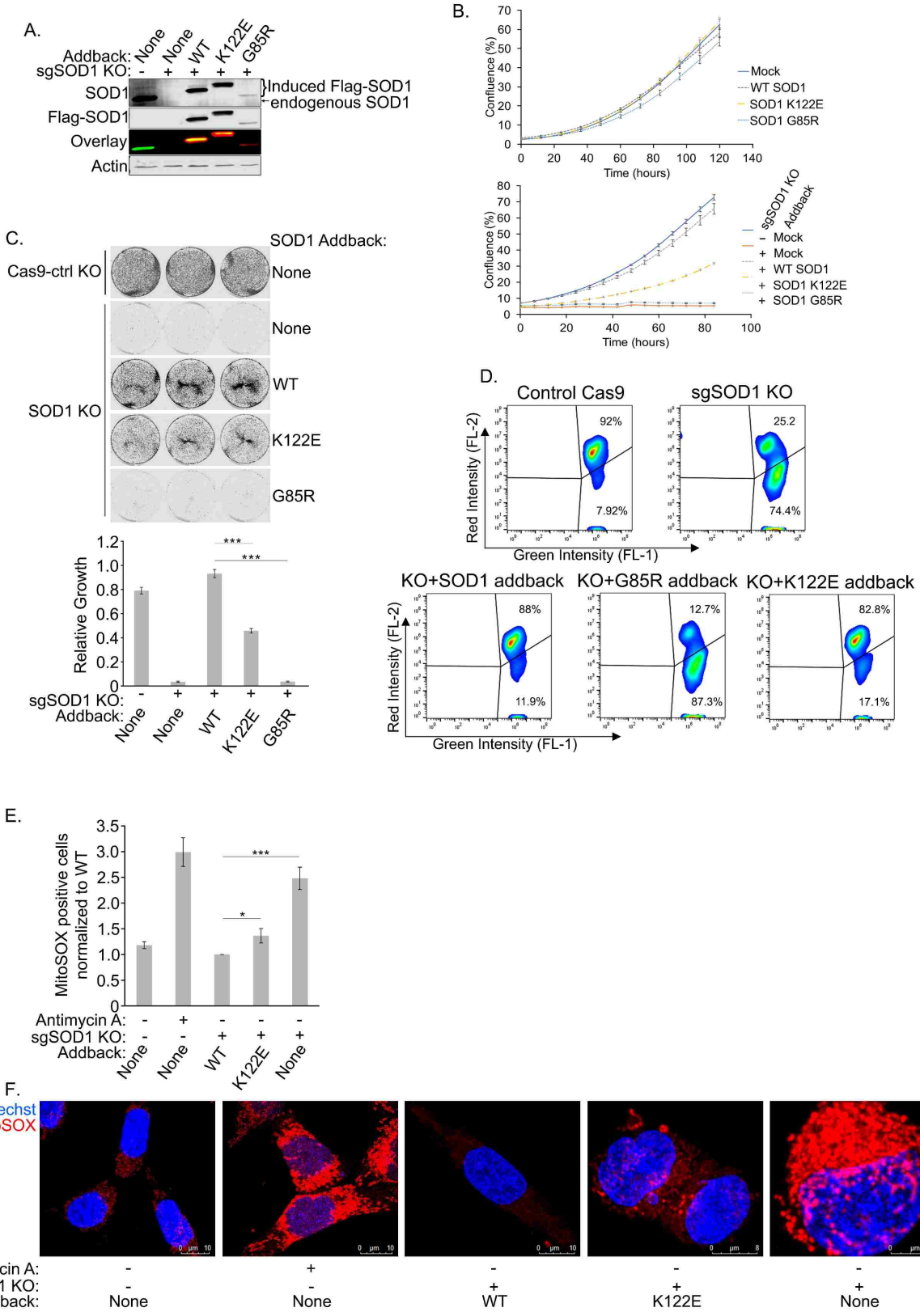
A.
Addback: None None WT K122E G85R
sgSOD1 KO: - + + + +
SOD1
Flag-SOD1
Overlay
Actin
Induced Flag-SOD1
endogenous SOD1
B.
Confluence (%)
Time (hours)
Mock
WT SOD1
SOD1 K122E
SOD1 G85R
sgSOD1 KO Addback
- Mock
+ Mock
+ WT SOD1
+ SOD1 K122E
+ SOD1 G85R
C.
SOD1 Addback:
Cas9-ctrl KO
SOD1 KO
None
None
WT
K122E
G85R
Relative Growth
sgSOD1 KO:
Addback:
D.
Control Cas9
sgSOD1 KO
Red Intensity (FL-2)
Green Intensity (FL-1)
92%
7.92%
25.2
74.4%
KO+SOD1 addback
KO+G85R addback
KO+K122E addback
88%
11.9%
12.7%
87.3%
82.8%
17.1%
E.
MitoSOX positive cells normalized to WT
Antimycin A:
sgSOD1 KO:
Addback:
F.
Hoechst
MitoSOX
Antimycin A:
sgSOD1 KO:
Addback:
None
None
WT
K122E
None

Figure 7. The SOD1 K122E acyl mimic is impaired in its ability to rescue the lethality of SOD1 deletion and reduce mitochondrial ROS levels. (A) Endogenous SOD1 was knocked out of HCT-116 T-REx cells using the CRISPR-Cas9 system. Expression of Flag-tagged SOD1 (with a mutated PAM site) was induced in the T-REx cells with Doxycycline. The cells were lysed and subjected to SDS-PAGE before being immunoblotted for endogenous SOD1 and overexpressed Flag-tagged SOD1. **(B)** Upper: SOD1 HCT-116 T-REx cells were seeded in 24-well plates and grown in the absence of doxycycline. Cell confluence was measured by an Incucyte Zoom. Lower: SOD1 was knocked out as in (A) and plated and analyzed as in (B; upper). **(C)** After knockout of endogenous SOD1 and overexpression of Flag-tagged SOD1, the HCT-116 T-REx cells were seeded at 22,500 cells per well and allowed to grow for 4 days before being fixed and stained with Giemsa. The wells were then imaged and quantified. (n=3 technical replicates; ***p<0.001; error bars are represented by +/- SEM) **(D)** Cells prepared as in (B) lower panel were stained with JC-1 to measure mitochondrial membrane potential. A live-cell population was gated from FSC and SSC measurements, and FL-1 was plotted against FL-2. Higher FL-2:FL-1 ratio indicates higher (healthier) mitochondrial membrane potential. **(E)** Cells prepared as in (B) lower panel were stained with MitoSOX Red to measure mitochondrial superoxide content. A live-cell population was gated from FSC and SSC measurements, from which a population of singlets was identified and selected. A threshold for positive MitoSOX stain was set based on the unstained control and a ratio of BL-3-positive cells to singlets was calculated and normalized to WT-add back cells. Higher ratio indicates larger proportion of cells with superoxide present. (n=4; *p<0.05, ***p<0.001; error bars are represented by +/- SEM) **(F)** Cells prepared as in (B) lower panel were stained with 5 μM MitoSOX Red for 10 minutes, and nuclei were counterstained. Prior to MitoSOX staining, positive control cells were treated with 30 μM antimycin A for 40 minutes.

effects of the sgRNA. As a control, the G85R mutant, which shows reduced ROS scavenging and does not inhibit respiration, was unable to rescue the growth defect in the SOD1 KO cells. In contrast, SOD1 K122E, which is ROS scavenging-active but defective in inhibition of respiration, showed an intermediate rescue of growth. JC-1 staining for mitochondrial membrane potential showed a similar trend with a dramatic loss of membrane potential, a hallmark of oxidative stress, in the SOD1 KO and G85R addback lines and a partial rescue of mitochondrial function in the

K122E-expressing cells (Figure 7D). To measure ROS levels directly within the mitochondria of each treatment, we used the MitoSOX mitochondrial ROS probe. Flow cytometric quantitation of mitochondrial ROS mirrored the proliferation and JC-1 results, with WT SOD1 rescuing the increase of mitochondrial ROS caused by SOD1 KO, and the K122E mutant showing a partial rescue (Figure 7E). Representative confocal images of this experiment are shown in Figure 7F. Together, these data suggest that SOD1-mediated dampening of respiration contributes to SOD1-mediated cell survival. Possible mechanisms to explain this effect are discussed below.

DISCUSSION

We began this study with several affinity purification-based proteomics approaches to identify PTMs across multiple tissues with the primary goal of finding new mechanisms of regulation on cell survival signaling nodes. All proteomics data from this effort is freely available (see link below under proteomics description). By using the machine learning approach of SAPH-ire (39), we prioritized several SOD1 PTMs for future study. Notably, a phosphorylation at S98 (or S99 depending on numbering scheme) showed the highest SAPH-ire score. This phosphorylation sits within a solvent-exposed beta sheet of SOD1 and has been shown to regulate SOD1's role in transcription (7). It is also notable that seven SOD1 PTMs were grouped within a high SAPH-ire score cluster, and all sit within a relatively small region spanning S98 to K128, which includes part of the electrostatic loop.

We focused our initial studies on an acetylation within the electrostatic loop of SOD1 at K122. This lysine was intriguing for several reasons. First, of the acylated lysines within the top SAPH-ire cluster, it had the highest number of independent MS identifications (Figure 2A). Second, it was conserved across multicellular eukaryotes and positioned within a known functional

domain of SOD1. Third, we had previously identified this lysine as a Sirtuin substrate using a biotin-switch approach in *Xenopus* egg extract (35), so its appearance in our proteomics data from mouse tissue was striking. Lastly, during the course of this project, Lin and colleagues confirmed the site as succinylated, which corroborated the lysine as a potentially important site of regulation, as lysines that are acetylated are also commonly succinylated (55).

Two observations shed light on the potential mechanism by which acylation at K122 inhibits SOD1-mediated suppression of respiration. First, we found that the ROS scavenging-impaired SOD1 G85R mutant fails to suppress respiration, which agrees with data from yeast that ROS-scavenging enzymatic activity is required for this new SOD1 function (13). Second, we found that the acyl-mutants of SOD1, K122E and K122Q, fail to suppress respiration yet have fully functional ROS scavenging enzymatic activity, which we confirmed through multiple assays. In aligning these two observations, we reasoned that acylation at K122 may disrupt a protein-protein interaction critical for suppressing respiration. Based on data from yeast, a clear candidate SOD1 interactor is CK1γ (13). Unlike its yeast counterpart, human CK1γ has no clear analogous C-terminal degron and we were unable to see the interaction by co-IP in human cells (limited by antibodies with poor specificity). However, there are several isoforms of human casein kinase and, interestingly, a sequence roughly matching the yeast CK1γ degron exists in the alpha isoform. Ongoing efforts are exploring these possibilities. Furthermore, we attempted unbiased co-IP proteomics to identify proteins that differentially interacted with SOD1 WT versus the K122E mutant, but these provided strikingly few proteins (data not shown). In consulting with others in the SOD1 field, this appears to be a fairly common observation and may indicate the need for cross-linking or other approaches to stabilize SOD1-interacting proteins for capture. Nevertheless,

our data support the idea that K122 acylation disrupts a SOD1 interaction that is critical for suppression of respiration and our future efforts will focus on this mechanism.

In searching for a mechanism to explain the ability of K122 acylation to regulate SOD1's anti-respiratory activity, we found that acyl-mimicking SOD1 mutants differed from WT SOD1 in that they failed to accumulate in mitochondria. This result initially led us to think that the acyl-K122 mutants failed to suppress respiration because they were unable to accumulate within the IMS, where we presumed they were directly inhibiting the ETC. However, we found that forcing the K122E mutant into the IMS with an IMS-targeting tag failed to recover its ability to suppress respiration. In addition, the IMS-targeting tag did not confer additional respiration-suppressing activity to WT SOD1. Nevertheless, this initially surprising result actually agrees with data from Reddi and Culotta, in which they showed that yeast SOD1 suppresses mitochondrial respiration from the cytosol by interacting with and stabilizing CK1γ (13).

Our observation that forcing the K122E mutant back into the mitochondria failed to recover its ability to suppress respiration caused us to reconsider how SOD1 acylation and IMS accumulation could be linked. Previous work suggests that the import of SOD1 into the IMS depends on an Erv1/Mia40 disulfide relay system (reviewed in (67)). The activity of this disulfide system is dependent on the oxidation of Erv1 by oxidized cytochrome c (74, 75). Therefore, under conditions in which respiration is highly active, the ratio of reduced-to-oxidized cytochrome c should increase, leading to a corresponding decrease in Erv1 oxidation and SOD1 mitochondrial import. Conversely, a drop in respiration (causing a build-up of oxidized cytochrome c) would increase SOD1 import into the IMS. In support of this model, we found that inhibiting respiration led to accumulation of SOD1 in mitochondria fractions, while boosting respiration with galactose caused a decrease in mitochondrial SOD1. Similar results have been observed in astrocytes (76).

Taken together with the IMS phenotype of the acyl-SOD1 mutants, we favor the model that acylation of SOD1 is upstream of SOD1 import into the IMS. Acylation of SOD1 blocks its anti-respiratory function, which in turn decreases its import into the IMS. Conversely, we posit that SOD1's ability to suppress respiration feeds forward to drive its own IMS import and acylation may serve as a brake on this mechanism.

In the bigger picture, an intriguing implication of this model is a potentially expanded view of SOD1-mediated anti-oxidant defense--That SOD1-mediated suppression of respiration contributes to its antioxidant/pro-survival function (see model in Figure 8). This could occur through at least two possible mechanisms: 1) Inhibition of respiration drives SOD1 into the mitochondria, placing SOD1 directly in position to scavenge ROS as it leaks from complex III. In support of this idea, elevated mitochondrial SOD1 increases cell viability in a yeast system (73) and mitochondria-targeted SOD1 rescues the loss of mitochondrial density observed in SOD1 null mice (72). This model is intriguing as a variety of stresses, such as ischemia/reperfusion and cell toxins, place strain on mitochondrial respiration and are known to cause spikes in mitochondrial ROS (77). 2) Alternatively, the dampening of respiration at complex I by SOD1 may inhibit ROS production directly. Interestingly, genetic inhibition of respiration partially rescues the loss of viability caused by SOD1 deletion in yeast (78). Furthermore, metformin is known to suppress mitochondrial ROS via inhibition of complex I (79-81). Exactly how this may occur is more puzzling as our understanding of ROS generation from the ETC, and complex I in particular, is limited. Prevailing dogma suggests that complex I only releases ROS into the matrix, but depending on the point at which complex I is inhibited, it could dampen the reduction of semiquinones or Fe-S clusters that may generate O_2^- elsewhere (82) or may simply reduce the flow of electrons to complex III, a key producer of ROS within the IMS (77).

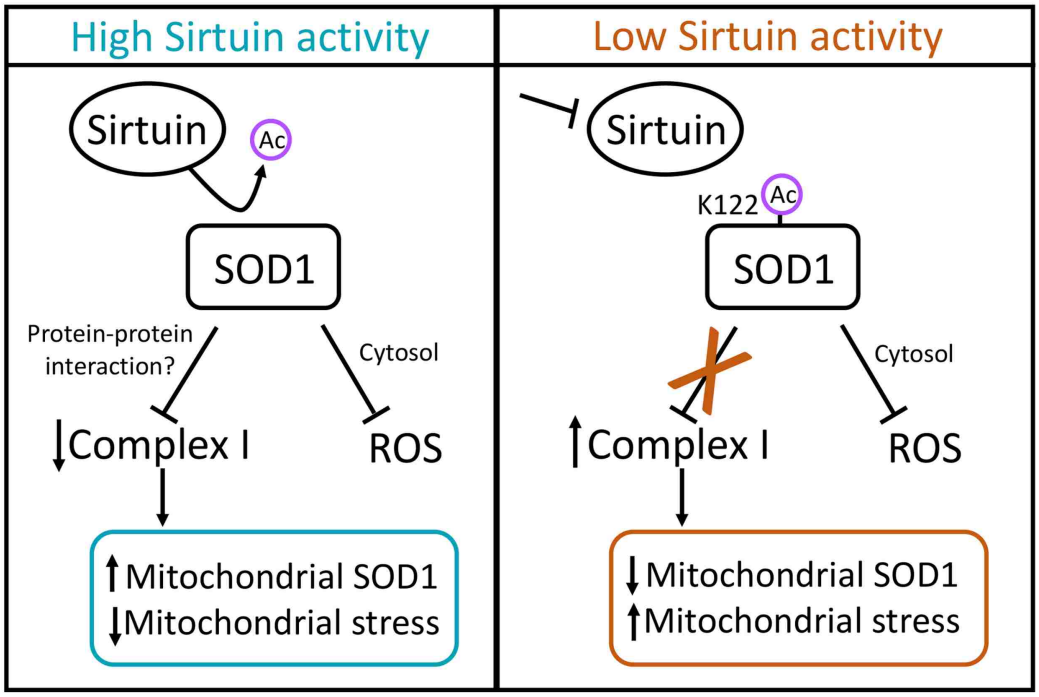

Figure 8. Model: High levels of Sirtuin activity (SIRT5 for SOD1 succinylation) deacylate SOD1, which activates SOD1's respiration-suppressing activity at complex I. We posit that SOD1-mediated inhibition of respiration contributes to SOD1-mediated cell survival through two potential (non-mutually exclusive) mechanisms: 1) Inhibition of respiration increases the mitochondrial pool of SOD1, placing SOD1 directly in position to scavenge ROS leaking into the IMS; 2) Dampening of respiration may directly reduce the production of ROS from the ETC.

We found that the impaired growth of SOD1 null cells, known to be caused by accumulation of oxidative damage (27, 44, 45, 50, 78), could only be partially rescued by the SOD1 K122E mutant, which is catalytically active against ROS but defective in inhibiting respiration. Taken together, our data suggest that SOD1-mediated inhibition of respiration, while clearly not the entire picture, may contribute to SOD1-mediated cell survival. Furthermore, the link between IMS import of SOD1 and respiratory activity suggests a feedback loop in which additional SOD1 may be recruited into mitochondria under conditions (e.g., mitochondrial damage leading to ROS production) in which reinforced ROS scavenging would be needed.

In summary, our data identifies, to our knowledge, the first acylation on SOD1 that regulates its ability to suppress mitochondrial respiration. Given that Sirtuin activity is linked to NAD^+ levels, which, in turn, are linked to the overall metabolic state of the cell, SOD1 acylation may act as a sensor to link nutrient metabolism to SOD1-mediated suppression of respiration. As described above, this may provide an additional dimension to SOD1 antioxidant defense. These data raise additional questions: Does SOD1 acylation disrupt a protein-protein interaction that transmits the signal to complex I? Given that our data suggest that dampened respiration promotes SOD1 mitochondrial import, could the toxic mitochondrial accumulation of ALS-linked SOD1 mutants in neurons be caused by an underlying perturbation of mitochondrial metabolism in a feed forward loop? Answers to these and other related questions will help shed light on the increasingly complex picture of SOD1 biology.

CHAPTER 3: INSIGHTS INTO SOD1 AND AUTOPHAGY

INTRODUCTION

Macroautophagy (more generally referred to as autophagy) is a cellular recycling process. Autophagy functions by engulfing targeted cargo with a single or double-walled membrane, fusing with a lysosome, and degrading its contents, leaving basic building blocks and nutrients to be used in new processes. It is associated with several identified roles in cell maintenance. For example, Autophagy has been shown to support immune and inflammatory responses in multicellular organisms (83). Kroemer, Marino, and Levine give an excellent review of the importance of autophagy in response to a host of cellular stresses (84). In essence, autophagy plays an assistant role to the proteasome and represents about 10% of total cellular protein/waste clearance with the proteasome accounting for the other 90% (85). Interestingly, although there is some overlap in cargo, the proteasome targets smaller, short-lived proteins while autophagy functions in turnover of large to massive, longer-lived proteins (85). For example, autophagy targets misfolded proteins, damaged protein complexes such as ribosomes, protein aggregates, and even whole organelles including mitochondria (85).

Given the importance of autophagy in maintaining healthy cell function, it follows that deficiencies in the autophagic program are problematic and can lead to cellular dysregulation or disease. Indeed, inadequate or excessive autophagic activity have been implicated in Parkinson's, Huntington's, Alzheimer's, and Lou Gehrig's diseases (86-90). And although autophagy does play a role in protecting organisms from tumor cell transformation, beyond a specific stage in tumor development autophagy can enhance tumor cell survival in nutrient-deficient conditions (91).

Autophagic flux can be estimated by several methods, including but not limited to measuring relative levels of Microtubule-associated protein 1A/1B-light chain 3 (LC3) (an extensive review on autophagy monitoring can be found in (92)). LC3-I is a soluble, 17 kDa protein found in the cytosol. In an active autophagy scenario, LC3-I is converted to LC3-II when it is covalently lipidated and inserted into the autophagosomal membrane. LC3-II is then degraded with the rest of the autophagolysosomal cargo (93). Therefore, if the rate of LC3-II degradation is controlled for or inhibited, the ratio of LC3-II to LC3-I indicates relative levels of autophagy flux. Another method to track autophagic activity was demonstrated by Weerasekara et al., wherein phospho signal at Ser 761 of ATG9a is indicative of active autophagy (94).

Autophagy can break down at several points whether chemically or physiologically, leading to autophagic deficiencies. For example, there are several known chemical inhibitors of autophagy that disrupt the process at early, mid, and late stage autophagy by known and unknown mechanisms (95). In biology, however, it can be less clear how and why autophagy fails. For example, several groups have shown that while effective and necessary for clearing aggregates and inclusion bodies of alpha synuclein, beta amyloid and tau, huntingtin, and SOD1 as in Parkinson's disease, Alzheimer's disease, Huntington's disease, and Lou Gehrig's disease (ALS), respectively, autophagy can lead to undesired cellular outcomes (86-90).

Autophagy can break down at several points whether chemically or physiologically, leading to autophagic deficiencies. For example, there are several known chemical inhibitors of autophagy that disrupt the process at early, mid, and late stage autophagy by known and unknown mechanisms (95). In biology, however, it can be less clear how and why autophagy fails. For example, several groups have shown that while effective and necessary for clearing aggregates and inclusion bodies of alpha synuclein, beta amyloid and tau, huntingtin, and SOD1 as in Parkinson's

disease, Alzheimer's disease, Huntington's disease, and Lou Gehrig's disease (ALS), respectively, autophagy can lead to undesired cellular outcomes (86-90).

Our preliminary results, though few, align with this information, and we offer additional evidence to support the role of autophagy in cellular maintenance in the context of an ALS clinical SOD1 mutant, SOD1 G93A. This chapter is highly preliminary in nature and represents a simple groundwork for future experiments in the Andersen Lab. In this work, we find that overexpressing G93A SOD1 with a second mutation (K122E) attenuates SOD1 mitochondrial localization, and restores lower ATG9a pS761 levels seen in WT SOD1 expressing cells. We find by size exclusion chromatography that both G93A and G93A/K122E SOD1 form high molecular-weight complexes compared to WT, offering evidence that aggregate toxicity may be exerted from within the mitochondria. We observe that mitochondrial content is reduced in G93A but not WT or G93A/K122E SOD1 expressing cells. Finally, by combining heavy water labeling with TOF LC-MS/MS we determine that overall protein turnover rates are increased in SOD1 G93A expressing cells compared to WT SOD1 overexpression. Together, these results point to SOD1 accumulation as sufficient to boost cellular autophagy, particularly when SOD1 localizes to and aggregates in the mitochondria.

RESULTS

Having previously established that WT SOD1, the deacyl-mimic K122R, and G93A SOD1 tended to localize to the mitochondria and that the SOD1 K122E succinyl-mimicking and K122Q acetyl-mimicking mutants remained in the cytosol (see chapter 2, Figure 6A), we thought it worthwhile to test the robustness of the effect of the K122 acyl-mimic mutations on SOD1 G93A mitochondrial localization. We overexpressed WT, G93A, G93A/K122R, G93A/K122E, and

G93A/K122Q SOD1 and after 48 hours, lysed the cells and enriched for mitochondria. To our surprise, Western blot analysis revealed that the G93A/K122E and G93A/K122Q double mutants showed highly reduced mitochondrial localization compared to G93A, G93A/K122R, and WT SOD1 (Figure 1), indicating that the localization effect of K122 acylation is significant and robust.

To more reliably measure the effects of SOD1, we developed isogenic cell lines with (in addition to an endogenous locus) a single inducible locus for WT, K122E, G93A, and G93A/K122E double mutant SOD1. In these cells, expression of SOD1 was under the control of a tetracycline-inducible promoter. We verified by immunoblot analysis that continuous induction over a time course led to continued increase of SOD1 expression. Interestingly, we observed that from equal quantities of cell lysate, at 72 hours of induction and beyond, WT SOD1 levels stayed constant but beta actin levels decreased (data not shown). Given that beta actin is a long-lived protein, this piqued our interest and led us to explore the possibility that autophagy was highly active in these cells after prolonged overexpression of SOD1. To measure autophagic activity, T-REx 293 SOD1 Flp-In cells were transfected with HA-ATG9a. At the time of transfection, cells were also treated with tetracycline to induce expression of WT, G93A, and G93A/K122E (double mutant) SOD1. After 48 hours, we immunoprecipitated HA and measured ATG9a pS761 levels with a 14-3-3ζ phospho-binding motif antibody validated for measuring pS761 levels on ATG9a (94). As shown in Figure 2, phospho signal was elevated in SOD1 G93A-expressing cells compared to WT. Of note, the double mutant showed a marked reduction of pS761 ATGa, more so than for WT SOD1. Given the differential tendencies of these SOD1 constructs to localize to the mitochondria or stay in the cytosol, these data strongly suggested that SOD1 aggregation was activating higher autophagy levels when it occurred in the mitochondria. This would imply that

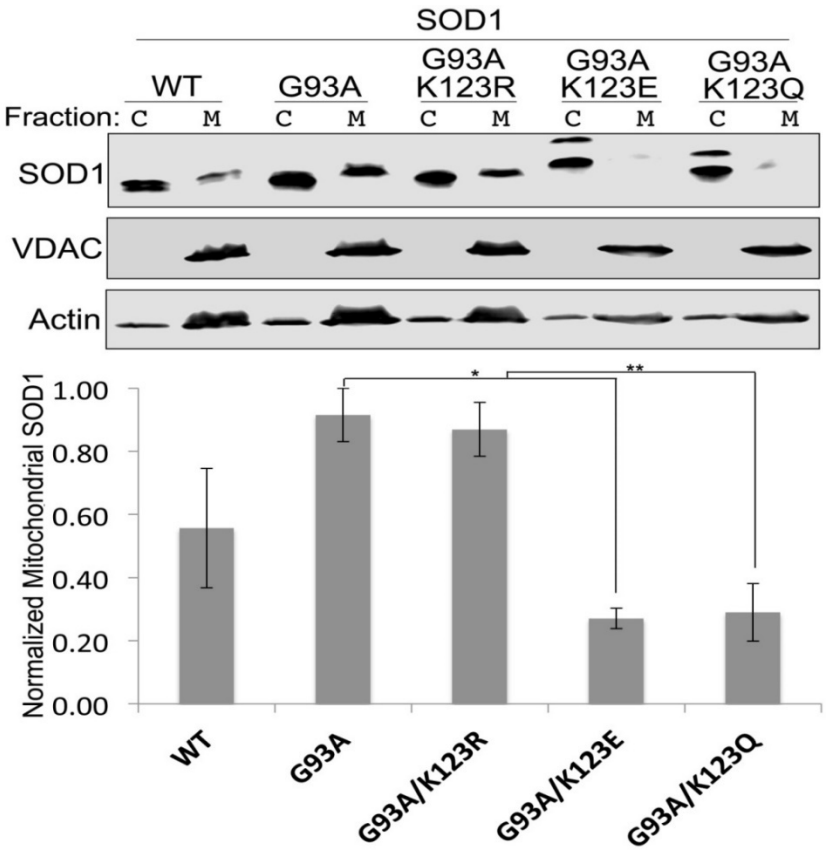

Figure 1. K122E succinyl-mimic mutation reverses mitochondrial localization of SOD1 G93A. HEK 293 cells were transfected with Flag-tagged WT, G93A, G93A/K122R, G93A/K122E, or G93A/K122Q SOD1. The cells were lysed and mitochondria were fractionated from the cytosol. The two fractions were run through SDS-PAGE and immunoblotted for Flag-SOD1 present in the mitochondria vs. the cytosol. (n=3 technical replicates; *$p<0.05$, **$p<0.01$; error bars are represented by +/- SEM)

the effect of the K122E mutation, in the context of G93A, is limited to SOD1 localization, and does not influence the propensity of G93A SOD1 to aggregate.

To test this idea, we induced expression of WT, G93A, and G93A/K122E SOD1 for 48 hours, lysed the cells, and subjected them to gel filtration analysis. Indeed, Western blot analysis of the gel filtration fractions showed both G93A and G93A/K122E SOD1 eluting in high-molecular weight fractions, compared to WT and endogenous SOD1 (see Chapter 2 Figure 6B). Given our data showing G93A SOD1 localized heavily to the mitochondria, and

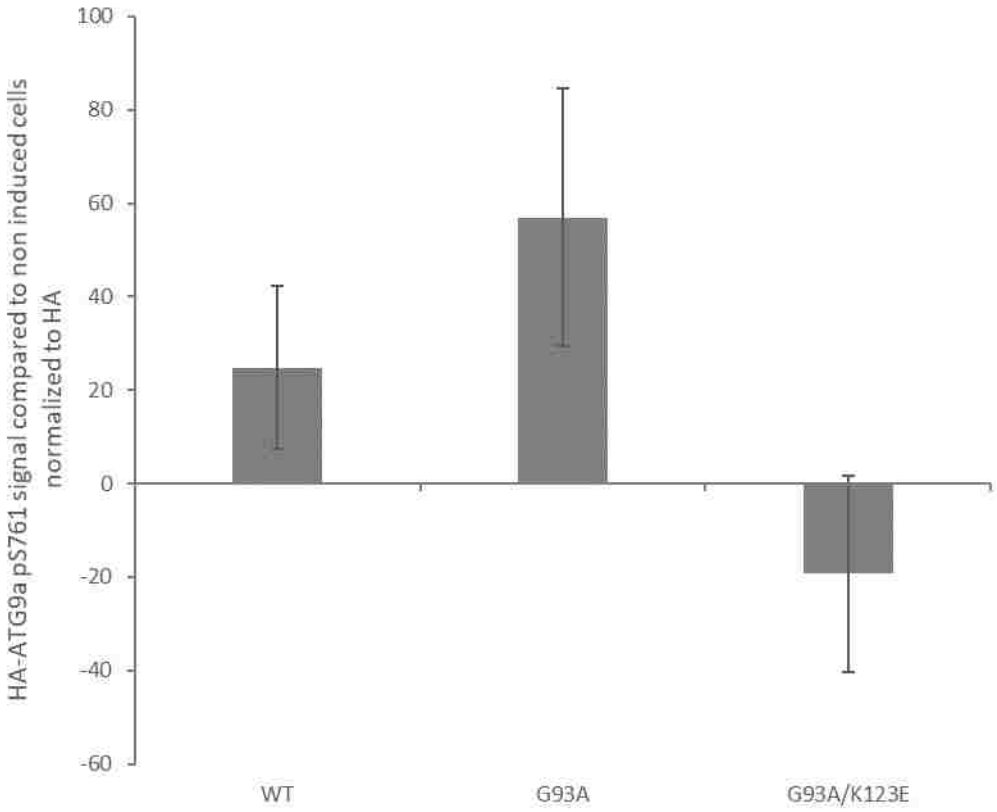

Figure 2. K122E succinyl-mimic mutation rescues lower ATG9a pS761 levels of SOD1 G93A. T-REx 293 SOD1 Flp-In cells were transiently transfected with HA-ATG9a. At the same time, cells were treated with tetracycline to induce expression of WT, G93A, or G93A/K122E SOD1. After 48 hours, cells were harvested, lysed, HA was immunoprecipitated, and ATG9a pS761 levels were measured by Western blot. (n=3 replicates; error bars represent +/- SEM)

G93A/K122E SOD1 primarily in the cytosol, these data suggest that the location of SOD1 aggregation does matter. They also suggest that the autophagy program being activated was one targeted specifically to mitochondria—a process known as mitophagy.

To further determine whether mitophagy was the main autophagic mechanism at play, we looked for a method to measure total cellular mitochondrial content. Complex IV of the mitochondrial electron transport chain (ETC) is composed of many conserved subunits, one of which is cytochrome c oxidase subunit 2 (MTCO2), thus making it a reliable readout for relative

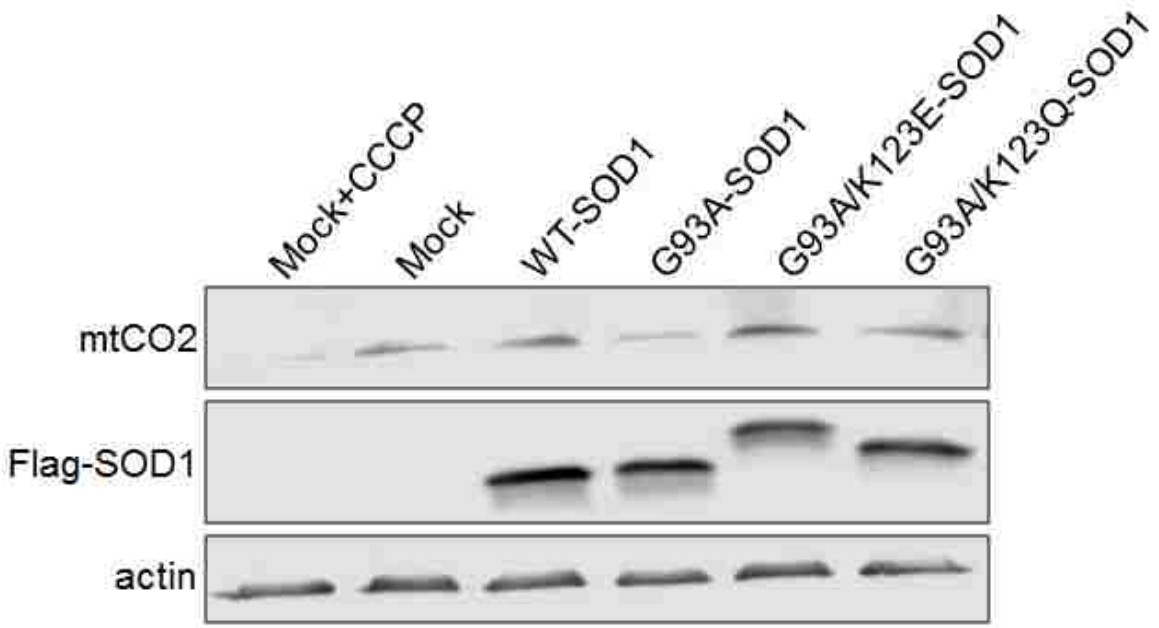

Figure 3. Mitochondrial content is reduced in G93A and K122 deacyl-mimic SOD1. HEK 293 cells were transiently transfected with WT, G93A, G93A/K122E, or G93A/K122Q SOD1, or with no DNA. Cells were harvested, lysed, and subject to Western blot analysis.

mitochondrial content within cell populations. We overexpressed WT, G93A, G93A/K122E, and G93A/K122Q SOD1 in HEK 293T cells and measured MTCO2 levels compared to a mock transfection and a positive mitophagy control population treated with CCCP, a known inducer of mitophagy (96). Western blot analysis revealed that in the mock, WT, and double mutant cells, mitochondrial content was relatively equal, compared to a marked reduction of MTCO2 in the CCCP and G93A SOD1 populations (Figure 3). These data indicate that the G93A SOD1 expressing cells have reduced mitochondrial content, suggesting that the mitochondria in those

cells are being subjected to a degradative process. This conclusion, however, is limited in that we have only a single measurement. Several more replicates would greatly assist in drawing a reliable conclusion.

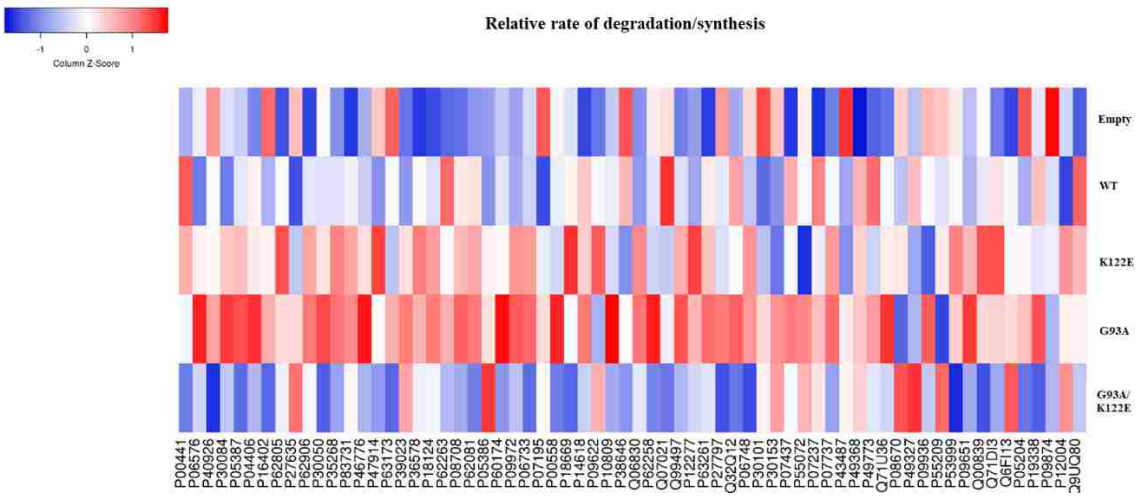

Figure 4. D_2O labeling coupled with LC-MS/MS reveals increased protein turnover rates in SOD1 G93A expressing cells compared to WT SOD. T-REx 293 SOD1 Flp-In cells were treated with tetracycline for 24 hours to induce expression of WT, K122E, G93A, and G93A/K122E SOD1. Cells were then treated with DMEM containing 5% deuterium oxide (v/v) and cells were harvested at time points of 0, 8, 16, and 24 hours of D_2O treatment. Cells were lysed and lysates were prepared for mass spectrometry analysis. Protein turnover rates were determined by an in-house modification of DeuteRater. See Methods for more detail. Red color indicates higher ratio of degradation/synthesis rates; blue color indicates lower ratio of same rates. White represents anything between lower and higher extremities.

To more precisely detect mitochondrial turnover in these cells, we used a novel method for tracking total protein production and degradation rates across several time points, developed by the J. C. Price Lab and based on heavy water labeling coupled with time-of-flight LC-MS/MS. We induced expression of WT, G93A, K122E, and G93A/K122E SOD1, in addition to a control population, for 24 hours before labelling cells with 5% deuterium oxide (D_2O) in complete DMEM. At time point zero (just prior to addition of D_2O) we harvested and froze one set of cells, and then added D_2O to the remaining cells. We then harvested cells at 8, 16, and 24 hours for a total of four time points. This would give the cells time to double approximately one time, based on our measurements, thus allowing enough time and growth for an intermediate, but not

overwhelming, amount of protein labeling. Following harvest, cells were prepared for and subject to mass spec analysis. The resulting spectra were validated and analyzed with an in-house program (see Methods chapter) and subsequently quantified. The analysis unexpectedly revealed that, compared to WT, G93A SOD1 cells exhibited globally increased protein turnover rates, and not just increased mitochondrial protein rates (Figure 4), suggesting that mitophagy was active, but other forms of macroautophagy may also be active. These results, though unexpected, are not surprising given that we initially observed decreasing quantities of beta actin. Furthermore, they align with the elevated or lowered ATG9a pS761 levels we measured in the same cell lines (see Figure 2). Taken together, these results suggest that toxic SOD1 accumulation in the mitochondria is sufficient to activate a global program of cellular autophagy, including mitophagy, and that SOD1 accumulation may not be nearly as toxic if kept outside of the mitochondria.

DISCUSSION

In our efforts to better characterize the robustness of the SOD1 K122E succinyl-mimic in keeping SOD1 out of the mitochondria, we found that succinylation has the potential to abrogate SOD1 G93A localization to the mitochondria almost entirely. However, we found that SOD1 G93A and the G93A/K122E double mutant both still aggregate. What is intriguing is that between the two, only G93A SOD1 increases autophagic activity. Therefore, we conclude that the location of the accumulation is crucial in determining whether or not the protein accumulation is toxic. It would be even more enlightening to look at survival and growth rates of cells with this model to further assess toxicity.

Furthermore, the D_2O-mass spectrometry data show an overall increase in protein turnover rates in G93A SOD1-expressing cells, which aligns with our measured increase in ATG9a pS761

signal. While many investigators have observed stalled or deficient autophagy in neurodegenerative models, it is reasonable to argue that our work actually agrees with the overall picture because in order for autophagy to become overwhelmed it must arguably be overactive first. Our work may more accurately represent the beginning stages where autophagy is overactive, given that we only overexpress SOD1 for 48 to 72 hours. This amount of time might be insufficient to mimic a late stage ALS patient or mouse model.

It is important to note that the initial connection we made between SOD1 and autophagy was based on extended overexpression of WT SOD1, and not the G93A clinical mutant. We have not looked at ATG9a pS761 levels in that context, but that would be valuable. If it was indeed increased autophagy activity that caused the observed decrease in actin, this would strengthen our working hypothesis that autophagy can be initiated globally as a result of mitochondrial protein overload; indeed, both WT and G93A SOD1 localize to the mitochondria. However, more work would need to be done to characterize which types of autophagy are activated in response to mitochondrial stress, given that our initial observation was decreasing actin. It would be useful to measure indicators of other forms of autophagy, such as ribophagy, to more correctly characterize the mechanisms induced by mitochondrial accumulation of SOD1.

Finally, the fact that the double mutant can reduce mitochondrial SOD1 import and rescue autophagic deficiencies suggests that we have a potential tool for mitigating the toxic effects of mutant SOD1 in fALS. If the experiments can be repeated with fidelity and show statistical significance, we could have a method to reduce or delay the proteotoxic effects observed in some neurodegenerative diseases that include SOD1.

CHAPTER 4: DISCUSSION

The importance of lysine acetylation and succinylation have recently emerged, especially in the context of cellular and metabolic regulation. These, along with phosphorylation and other post-translational modifications (PTMs) have proven to be the means of integrating complex metabolic signals in a rapid, adaptive manner. Given the overwhelming evidence that metabolic dysregulation frequently leads to disease, we initially set out to identify specific PTM-regulated proteins, and to find where those modifications were happening. Our proteomics results revealed several candidates, including SOD1. Indeed, our overall results identified SOD1 as a protein with a PTM-driven regulatory mechanism. Specifically, acetylation- and succinylation-mimicking mutations (acylation) of SOD1 K122 abolish the ability of SOD1 to repress respiration and prevents its import into the mitochondria, without perturbing canonical SOD1 antioxidant function. Furthermore, based on our cell growth/survival, mitochondrial membrane potential, and mitochondrial ROS measurements, we observed that deacylated SOD1-mediated suppression of respiration resulted in improved mitochondrial health/function and promoted resilience to stress. Therefore, acylation of SOD1 K122 represents a potential and novel target for treatment of SOD1 pathologies. However, more work is required before those strategies can be developed.

Interestingly, in contrast to the beneficial effects observed in WT SOD1-expressing cells, wherein SOD1 localizes to the mitochondria, G93A SOD1 which also accumulates in the mitochondria, has shown an opposite effect in G93A mouse models. These models are well known to develop symptoms identical to an ALS patient, including motor neuron death, and eventual mortality. Therefore, it is possible that within a cell, it may be part of a survival or defense mechanism to import SOD1 into the mitochondria under stressed conditions, however if that SOD1 is prone to aggregate, as with the G93A mutant, this could lead to unintentional and irreversible

toxicity. Indeed, our data show decreased mitochondrial content and increased autophagic flux when SOD1 G93A is overexpressed, suggestive of just such irreversible mitochondrial damage, assuming mitochondria are being engulfed and degraded through autophagy. Furthermore, given that WT SOD1 represses respiration, and that our data suggest that dampened respiration promotes SOD1 mitochondrial import, it is possible that any folded G93A is also repressing respiration, which would drive more SOD1 into the mitochondria in an irreversible feed forward loop. This contrasts with WT SOD1, which does not aggregate.

It is clear from our data that SOD1 exerts its regulatory effect on respiration upstream of import into the mitochondria, however as mentioned in Chapter 2, the underlying molecular mechanism is unknown. It is possible that altering the acyl state of SOD1 K122 introduces steric hindrance or a conformation change sufficient to preclude an interaction with putative binding partners involved in respiratory signaling. For example, as hinted at in the Discussion in Chapter 2, SOD1 in yeast binds to the C-terminal degron of casein kinase 1 gamma (CK1γ), which propagates the anti-respiratory signal through the Wnt signaling pathway. And in mammalian cells, the alpha isoform of CK1 has a similar degron sequence. It is possible, then, that SOD1 could bind to the alpha isoform. However, this may not be the case given that in the yeast ortholog, SOD1 entirely lacks a lysine at the relative aligned position (see Figure 2F in Chapter 2).

To study the interaction of SOD1 with CK1, we plan to use an overexpression system with three isoforms of CK1 coupled with mass spectrometry, immunoprecipitation, and confocal microscopy. As previously mentioned, SOD1 shows a limited number of interactors when subject to immunoprecipitation and mass spectrometry, therefore we may need to include a crosslinking step in those experiments. Alternatively, we have developed a BirA-SOD1 construct that expresses a BioID-SOD1 fusion protein capable of biotinylating any proteins that come within proximity of

SOD1. This would enable a streptavidin-based immunoprecipitation of proteins that potentially interact with SOD1, whether transient or long-term. Immunoprecipitated targets could then be analyzed via mass spectrometry and Western blot. This strategy may provide a reliable method for revealing SOD1 interactors, including any involved in regulating mitochondrial respiration.

In Figure 7 of Chapter 2, we examine the effects of different acyl-mimicking forms of SOD1 K122 on cell growth and survival via a knock-out/add-back approach. It would be valuable to KO endogenous SOD1 in the T-REx Flp-In SOD1 CytB2 K122E cell line as well as in CytB2 WT SOD1, induce expression of these mitochondria-targeted SOD1 constructs, and see whether growth phenotypes more closely resemble those of WT or K122E SOD1.

In chapter 2 we address the effect of depleting SIRT5 on endogenous levels of SOD1 K122 succinylation. In light of the growth and survival studies conducted in the T-REx HCT-116 Flp-In SOD1 system, it would be informative to repeat those experiments in just the WT SOD1 cells, in the presence or absence of SIRT5 interfering RNA. We would postulate that when SIRT5 is knocked down, cells would more closely resemble the K122E succinyl mimics. To accompany that study with fractionation and mitochondrial enrichment to measure localization of SOD1 would also be very informative. It seems likely that if SIRT5 were depleted, less SOD1 would be found in the mitochondria. And in this same system, it would be interesting to measure mitochondrial ROS levels in WT SOD1 cells with or without SIRT5 depletion. I would hypothesize that depleting SIRT5 would lead to increased mitochondrial ROS, similar to what was measured in SOD1 K122E expressing cells in Chapter 2 Figure 7E.

As yet, we do not know the clinical relevance of our results. To work towards that, we are conducting xenograft studies with mice inoculated with T-REx HCT-116 Flp-In SOD1 WT and

K122E cells. We anticipate that the SOD1 WT-treated mice will develop larger, more aggressive tumors, while those treated with SOD1-K122E cells should show tumors with a comparatively smaller volume. Preliminary feedback indicates that there may be issues with the way in which doxycycline is being administered (in food pellets), and that putting it in their water may be more effective. Final analysis and evaluation will be available soon.

Finally, as part of our initial efforts, a SAPH-ire based analysis (see Figure 2A-2D in Chapter 2) revealed that there are at least six more SOD1 residues that are modified by PTMs at high frequency within a biologically relevant region of SOD1. These residues will serve as a valuable platform for future SOD1 studies and may contribute even more insight into SOD1's complex mode of regulation.

CHAPTER 5: MATERIALS AND METHODS

Mass Spectrometry and PTM Affinity Purifications. Trypsin-digested cell lysates from mouse embryo, brain, and liver were prepared by lysis in 8 M urea, followed by normalization to approximately 2 mg/mL and 1.8 M Urea, reduced with 10 mM dithiothreitol, alkylated with 20 mM iodoacetamide, and digested with TPCK trypsin at 1:25 w/w. Peptides were desalted with C18 SPE cartridges (Waters) and lyophilized to dryness. Approximately 5 mg aliquots of each lysate digest was enriched for post-translational modifications using the PTMScan product line (Cell Signaling Technologies), including a series of phospho-specific motifs (AKT, MAPK, phosphothreonine, or pY) as well as ubiquitin remnant (GG-K), or acetyl-lysine (Kac), as previously described (97-99). Titanium dioxide enrichment was performed as previously described, for comparison (99).

After immunoaffinity or titanium dioxide enrichment, peptides were analyzed using data-dependent acquisition (DDA) by a 3-fraction LC/LC-MS/MS method as previously described (100). Samples were resuspended in 12 µl of 1/2/97 v/v/v TFA/MeCN/water. Phosphopeptide samples additionally contained 20 mM citric acid. Approximately half of each sample was analyzed on a 2D nanoAcquity UPLC coupled to a Synapt G2 HDMS (Waters Corporation). Searchable files (*.mgf) were generated from raw data in Mascot Distiller, and database searching for peptide ID and Mascot search engine v2.4 (Matrix Science, Inc.). The UniProt database (www.uniprot.org) with *mus musculus* taxonomy and reviewed status was utilized, along with 10 ppm precursor and 0.04 Da product ions. Fixed modification of Cys with carbamidomethylation was required, and variable modifications included deamidation NQ, oxidation M, along with acetylated K, ubiquitin remnant), or phosphorylated S/T/Y. Full tryptic specificity was required. Data was curated in Scaffold v4.7 using PeptideProphet algorithm, to a 0.05% peptide and 0.4%

protein FDR. The Scaffold file is available for download at https://discovery.genome.duke.edu/express/resources/3023/3023_PTMScanAll_withTiO2.sf3. All mouse experiments were IACUC approved.

SAPH-ire. SAPH-ire FPx was employed as described previously (39), with modifications for the domain-specific analysis of the superoxide dismutase (SOD) copper/zinc binding domain (IPR001424). FPx scores were calculated using the structure-free 8-factor neural network model as described previously (38). The SOD domain sequences for all eukaryotic proteins were obtained from Pfam (101). The multi-FASTA files generated for the domain family were subsequently aligned using MUSCLE with default parameters (102). The domain dataset for SOD contained 79 unique sequences within which 77 distinct PTMs could be retrieved from the public domain. PTMs coalesced into 34 modified alignment positions (MAPs) in the family, the features of which were used for SAPH-ire FPx scoring.

Cell Culture and Reagents. HEK 293T cells were purchased from ATCC. Flp-In T-REx 293 host cell line was purchased from Thermo Fisher Scientific (R78007). The Flp-In T-REx HCT-116 host cells were developed by Dr. Stephen Taylor (103). All cell lines were cultured in Dulbecco's modified Eagle's medium (DMEM, Gibco no. 11965) supplemented with 10% fetal bovine serum (FBS) at 37 ºC in a 5% CO_2 incubator.

Antimycin A (A8674), 3-Nitropropionic acid (3-NP) (N5636), galactose (G5388), tetracycline (T7660), doxycycline (D3447), and CCCP (C2759) were purchased from Sigma. Rotenone was purchased from Millipore (557368). Drugs used in cell culture were dissolved in the recommended solvent and then diluted in cell culture media to the indicated final concentrations.

Plasmid Transfections and siRNA. Cells were transfected with plasmid expression vectors pcDNA3.1, HA- or FLAG-SOD1, or HA-Atg9 (gift from Dr. Luigi Puglielli at the University of Wisconsin) with polyethylenimine (PEI, Polyscience Inc.) transfection reagent in a 1:3-4 (μg DNA:mg PEI) ratio. Site-directed mutants of FLAG-SOD1 were generated using the Agilent QuikChange II XL kit (200521) or the Q5 Site Directed Mutagenesis kit from New England Biolabs, Inc. (E0554). Plasmids and selection reagents for Flp-In T-REx host cell lines were obtained from Thermo Fisher Scientific. RNAiMAX Lipofectamine reagent was purchased from Invitrogen (13778100). Smartpool siRNA against SIRT5 was obtained from GE Dharmacon (M013448010005). The Cytochrome B2 SOD1 cDNA was obtained from Dr. Giovanni Manfredi.

Generation of Flp-In T-REx Cell Lines. Generation of T-REx cells lines with Flp-recombinase mediated gene insertion allows for tight control of expression of a gene of interest at a single, actively transcribed genomic locus by addition or removal of tetracycline or its derivatives. For further explanation, refer to the manufacturer's manual (Thermo Fisher Scientific no. R78007).

T-REx host cells were transiently transfected with pOG44 and pcDNA5/FRT/TO-FLAG-SOD1, including WT SOD1 and acyl-mimicking mutants, at a ratio of 9:1 (pOG44:pcDNA5). Constructs were co-transfected into cells in 6-well plates when cells were approximately 60% confluent. After 48 hours, cells were trypsinized and transferred to 15 cm cell culture dishes and cultured in complete medium containing 150 μg/mL of hygromycin B selection reagent (Gibco 10687010). After 10 days, single colonies were transferred to individual wells of a 24-well plate and cultured in medium without selection reagent. Plates were replicated and expression was induced for 24 hours with 1 μg/mL tetracycline in one set of the replicates, after which cells were harvested, lysed, and subjected to Western blot analysis as described below. Cells

positive for the FLAG epitope were selected, and cells with the lowest background expression when not induced, but still exhibiting high inducible expression with tetracycline, were selected for use in experiments. For experiments, expression was induced with either tetracycline or doxycycline at a final concentration of 100 ng/mL.

Antibodies. Primary mouse monoclonal anti-HA (7392), rabbit polyclonal anti-FLAG (807), mouse monoclonal and rabbit polyclonal anti-beta actin (8432, 1616) were purchased from Santa Cruz Biotechnology. Primary mouse monoclonal anti-FLAG (8146), rabbit polyclonal anti-FLAG (2368), mouse monoclonal and rabbit polyclonal anti-human SOD1 (4266, 2770), mouse monoclonal anti-HA (2367), rabbit monoclonal anti-SIRT5 (8779), rabbit polyclonal anti-VDAC (4661), and mouse monoclonal phospho-serine 14-3-3 binding motif (9606) were purchased from Cell Signaling Technology, Inc. Primary mouse monoclonal anti-GAPDH and rabbit monoclonal anti-MEK1/2 were purchased from Abcam (9484, 178876). Anti-mouse and anti-rabbit IRDye 680RD and IRDye 800CW secondary antibodies were purchased from Licor (92668070, 92632210, 92668071, and 92632213).

Succinyl-Lys122 Antibody Purification: Rabbits were immunized against the succinylated-SOD1 peptide (LVVHE[succinyl-K]ADDLGC) and serum was collected. Succinyl-Lys122 polyclonal antibody was immunopurified out of serum using succinylated Lys122 SOD1 peptide as previously reported (104). In brief, biotinylated (non-succinyl) Lys122 peptide was conjugated to streptavidin-agarose (20359, Thermo Scientific) and gently rotated at 4 ºC overnight with rabbit serum diluted 1:1 in equilibration buffer (150 mM Tris [pH 7.5], 20 mM NaCl) to deplete non-succinyl Lys122-specific antibody from serum. Following incubation, serum was transferred to a column containing succinylated Lys122 peptide conjugated to streptavidin resin and again incubated overnight with gentle rotating. Resin was thereafter washed twice with equilibration

buffer. Succinyl Lys122-specific antibody was then eluted from resin with elution buffer (0.1 M glycine-HCl [pH 2.8]) by gravity elution. Fractions were then collected in microfuge tubes and neutralized with neutralization buffer (1 M Tris-HCl [pH 8.5]). Reactivity of each fraction was tested via Western blot for antibody titer.

Primary anti-human SOD1 succinyl-Lys122 antibody serum, biotinylated SOD1 succinyl-Lys122 peptide, and biotinylated SOD1 non-succinyl Lys122 peptide were produced by Eton Bioscience, Inc.

Western Blotting and Immunoprecipitation. Cells were seeded in 10 cm or 6-well plates to 15% confluence. After 24 hours, at about 30% confluence, T-REx cells were induced, or non T-REx cells were transfected with a SOD1 expression vector, an empty vector, or mock transfected. After 8 hours, cell culture medium was replaced with complete medium and incubated at 37 ºC in a cell culture incubator until 48 hours post-transfection. Cells receiving drug treatment were treated within this incubation time at the indicated concentrations. Cells treated with RNA interference were transfected with 100 nM SIRT5-directed or scrambled siRNA with RNAiMAX Lipofectamine. The knock-down was repeated to ensure efficient depletion of SIRT5. Then cells were allowed to grow 24 to 48 more hours. Following transfection and incubation, cells were washed twice and harvested with ice-cold PBS. Cells were then lysed in ice-cold coimmunoprecipitation buffer (10 mM HEPES [pH 7.5], 150 mM KCl, 0.1% NP-40) or TNTE coimmunoprecipitation buffer (20 mM Tris [pH 7.8], 150 mM NaCl, 0.3% w/v triton X-100, 5mM EDTA), supplemented with protease inhibitors (88665 Pierce). Lysates were then cleared by centrifugation at 21,000 x g for 10 minutes at 4 ºC. Lysate protein concentration was determined by a Bio-Rad protein determination DC Assay (5000116). Lysate was saved for analysis or incubated with 15 µL of anti-FLAG-agarose resin (2220 Sigma). Protein was eluted from the resin

by incubation with modified Laemmli buffer for 5 minutes at 100 ºC. Lysates were likewise mixed and boiled in modified Laemmli buffer. Samples were then loaded onto SDS PAGE gels. Bluestain protein ladder (P007 GoldBio) was used as a molecular weight reference. Gels were then transferred to a PVDF membrane and immunoblotted for proteins of interest. Proteins were visualized and bands were quantified using the LI-COR Odyssey Classic or CLx imaging systems and Image Studio software package.

SOD1 Activity Assays. For the *in vitro* colorimetric activity assay, HEK 293T cells were transfected with a FLAG-SOD1 plasmid or mock transfected. Cells were harvested, lysed, and FLAG was immunoprecipitated with FLAG epitope-conjugated agarose beads, after which the resin was washed 3x in cold PBS. FLAG-SOD1 was then competitively eluted from the beads by incubation in a 200 ng/µL solution of purified FLAG peptide (Apex Bio), with gentle shaking for 10 minutes at 4 ºC. Beads were then centrifuged at 8,200 x g for 30 seconds at 4 ºC. The FLAG-SOD1-containing supernatant was transferred to a new microfuge tube and the elution was repeated and added to the same tube. With the purified SOD1 or mock supernatants, SOD1 ROS scavenging activity was indirectly measured using a SOD Assay Kit purchased from Sigma (19160), according to manufacturer's recommendations.

For the *in situ* SOD1 activity gel, purified FLAG-SOD1 was produced as in the colorimetric assay. SOD1 ROS scavenging activity was indirectly measured as a competitive reaction of superoxide with nitroblue tetrazolium (NBT) dye as previously described (105). Briefly, a portion of the purified SOD1 supernatants were mixed with 5x SOD loading dye (25 mM Tris-HCl [pH6.8], 50% glycerol, 0.5% bromophenol blue) to a final concentration of 1x loading dye. Samples were then loaded onto an 8% native PAGE gel and SOD1 was resolved at 80 V constant until the loading dye reached the end of the gel. The gel apparatus was maintained

at 4 ºC. The gel was then moved to a shallow container, immersed in 50 mL of staining solution (45 mM K_2HPO_4, 4.6 mM KH_2PO_4, 0.163 mM NBT, 0.266 mM riboflavin), and covered with foil. 50 µL of TEMED was then added and the gel was incubated with gentle shaking for 1 hour in the dark. Following incubation, the staining solution was removed and the gel was washed 2x with distilled water, and then immersed and incubated in distilled water with gentle shaking overnight, while exposed to ambient light. Clear bands on the blue-stained gel were interpreted as active SOD1. NBT (N6639), K_2HPO_4 (P3786), KH_2PO_4 (P0662), and riboflavin (R9504) were purchased from Sigma.

Cell Survival Assay. Single-guide RNA (sgRNA) against SOD1 was cloned into the pSpCas9(BB)-2A-Puro (PX459) vector. PX459 was a gift from Feng Zhang (Addgene plasmid # 48139) (106). Human codon–optimized Cas9 from S. *pyogenes* and the sgRNA were expressed from the human cytomegalovirus (CMV) immediate early promoter and the human U6 promoter, respectively. The SOD1-targeted 20 base pair sgRNA contained the sequence TTGCATCATTGGCCGCACAC with an NGG protospacer adjacent motif (PAM) site of TGG. Knock-out efficiency was measured via Western blot analysis. The construct was transfected into T-REx HCT-116 cells. After eight hours, transfection medium was removed and replaced with DMEM complete medium. 24 hours post-transfection, cell culture medium was replaced with DMEM complete medium containing 3 µg/mL puromycin selection reagent. After 48 hours, selection medium was removed and replaced with DMEM complete medium containing 100 ng/mL doxycycline. Doxycycline medium was replenished every 48 hours and cells were trypsinized as needed. Cells were allowed to grow until there were sufficient cells for the assays, after which cells were trypsinized and counted.

Growth Assay with Giemsa Stain: For Giemsa staining, 22,500 cells per well were seeded into 6-well plates with 100 ng/mL doxycycline and allowed to grow for 5 days. Cells were then washed twice with ice cold PBS, fixed for 30 minutes in ice cold methanol at 4 ºC, after which methanol was aspirated and a 1:20 mixture of Giemsa stain (Fluka Analytical 48900) to PBS was added to cells and incubated at room temperature for 45 minutes. Following staining, cells were washed 3 times with distilled water and allowed to air dry. Wells were imaged and quantified using the LI-COR Odyssey Classic imaging system and Image Studio software package.

Incucyte Zoom Analysis: For Incucyte analysis of control cells without SOD1 knockout, 12,500 cells were seeded per well into 12-well plates. For the SOD1 knockout/addback cells 18,000 cells were seeded per well into 24-well plates. Plates were put into the Incucyte one day after seeding and cell confluence was monitored via basic phase contrast analysis for 80 to 120 hours. Cell confluence was given as the mean of 4 wells per sample, 16 images per well. Error bars are represented as +/- SEM.

Cellular Respiration. HEK 293T cells were transiently transfected with 8 μg of a SOD1 plasmid, empty pcDNA3.1, or mock transfected. Eight hours later, cell culture medium was replenished and cells were allowed to grow for a total of 48 hours. For rotenone treatment, 1 nM rotenone or vehicle was added to HEK 293 cells 30 minutes prior to measuring oxygen consumption rates, and incubated at 37 ºC in 5% CO_2 atmosphere. Cells were then detached in culture dishes with 0.05 % trypsin–EDTA (Gibco) and growth medium was added to the culture. Contents were transferred to a 15 mL conical tube and centrifuged at room temperature. After removal of supernatant, the cells were permeabilized, prepared for the Oroboros O2K (Oroboros Instruments, Innsbruck, Austria), and O_2 flux was measured as previously described by Hodson et al. with the exception of a few changes as outlined below (107). The data presented is taken from

maximal O_2 flux measurements when the full electron transport system capacity of oxidative phosphorylation was measured after addition of FCCP. For the complex I and complex II inhibition assay, rotenone (2 mM) and malonate (2.5 mM) were added prior to O_2 flux measurements. After respiration was measured, cellular protein concentrations from the same cells were determined as in 'Western Blotting and Immunoprecipitation'. For the rotenone treated cells, 2 million cells were counted and assayed in the Oroboros O2K.

Endogenous Immunoprecipitation. Endogenous immunoprecipitation of SOD1 was performed using the Dynabeads Co-Immunoprecipitation Kit purchased from Thermo Fisher Scientific (14321D) according to the manufacturer's recommendations. To pull down SOD1, 7.5 mg of magnetic epoxy beads were conjugated to 37.5 µL of SOD1 antibody, per sample. As an IgG control for SOD1 immunoprecipitation, primary anti-Chk1 was conjugated to magnetic beads.

Mitochondrial Enrichment. All mitochondrial isolations were done with the Mitochondria Isolation Kit for Cultured Cells, obtained from Thermo Scientific (89874). Mitochondrial pellets were isolated according to manufacturer's protocol.

D_2O labeling for protein turnover-rate determination. T-REx 293 cells were seeded into 10 cm plates to 20% confluence and tetracycline was added to appropriate plates. At 40% confluence, time-zero samples were imaged, harvested, and cryo-frozen. For the remaining samples, cell culture media on all plates was replaced with DMEM complete medium containing 5% deuterium oxide. In addition, liquid in the 5% CO2 incubator water bath was replaced with 1 L of water containing 5% deuterium oxide to maintain D_2O at a 5% equilibrium in the cell culture medium. Over the next 24 hours, samples were imaged, harvested and cryo-frozen at designated 8, 16, and 24hr time points. One milliliter of cell labeled cell culture medium from each sample

and from the incubator water bath was saved to affirm constant 5% D_2O throughout the labelling period. Once all samples were harvested, cells were prepared for mass spectrometry analysis by filter-aided in-solution digest, as previously described (108) but with several modifications. Specifically, cells were lysed in 6 M guanidine-HCl (pH8.5) containing protease inhibitors. For full lysis, cells were incubated in lysis buffer with rotation at 4 °C, followed by homogenization by shaking on an MP FastPrep-24 (MPBio) with 3.0 and 1.3 mm stainless steel beads. Lysates were cleared by centrifugation at 21,000 x g for 20 minutes at 4 °C. Protein concentration of each sample was determined by a BCA assay, and 100 µg of each sample was transferred to a fresh screw-cap tube. Samples were reduced with 5 mM DTT for 5 minutes at 55 °C. Samples were cooled to room temp and then incubated in the dark overnight with 15 mM iodoacetamide. The following day, samples were transferred to 10 kDa MWCO filters and centrifuged at 14,000 x g for 30 minutes. Samples were washed and centrifuged twice with 100 µL 6 M guanidine (30-minute centrifugation at 14,000 x g), followed by two washes with 25 mM ammonium bicarbonate. After washing, filters were transferred to fresh collection tubes and 400 µL of 25 mM ammonium bicarbonate was added to the top of each filter. Mass spec-grade trypsin was then added to the solution above each filter at a 1:50 (w/w) ratio and samples were incubated with very gentle shaking at 37 °C overnight. The following morning, samples were centrifuged at 14,000 x g for 30 minutes, filtrant was collected and transferred to mass spec vials, samples were dry-lyophilized by vacuum centrifugation, and finally resuspended in mass spec buffer A (3% acetonitrile, 0.1% formic acid) to a final concentration of 1 µg/µL.

Samples were run on an Agilent Technologies 6530 mass spectrometer with a Chip-Cube source. Source used Agilent Technologies Polaris HR-Chip-3C18 as the column. Digested samples were subjected to a 27-minute gradient from 100% Buffer A (96.9% water, 3%

Acetonitrile, 0.1% Formic Acid) to 70% Buffer B (96.9% Acetonitrile, 3% Water, 0.1% Formic Acid), followed by a 5-minute wash with 95% Buffer B.

Data was analyzed using the SpectrumMill program from Agilent Technologies using the sixth release of the 2016 "Reviewed" Uniprot Homo sapiens taxonomy. Files were extracted, searched using trypsin as the protease with two missed cleavages allowed. Autovalidation was performed by SpectrumMill and then a no enzyme search was performed to identify unusual trypsin cuts. Both database searches were performed with a fixed modification of carbamidomethylation of cysteine and variable modifications including oxidation of methionine and pyroglutamic acid from N-terminal glutamine.

Data was prepared for quantification using a modification of the extractor module from DeuteRater (109). This in-house program takes the scans identified with DeuteRater's extractors, removes peaks 4 or more MS1 scans away from the main chromatogram and fills in any missing scans in the chromatogram. All the abundances from the first isotopic peak (no extra neutrons) to the 4th isotopic peak (3 extra neutrons) are then summed together. The resulting data was analyzed using InfernoRDN using the standard method (110). Heat map analysis was prepared through Heatmapper (111) using the expression analysis tool, without any clustering analysis.

SOD1 Aggregation Assay. T-REx HEK 293 with WT, G93A, or G93A/K122E SOD1 cells were plated at 20% confluence in two 15 cm plates per sample. Tetracycline was added to culture medium to induce expression of the SOD1 constructs, and cells were allowed to express for 48 hours. Tetracycline-containing medium was replenished after 24 hours due to tetracycline instability. Cells were washed twice with ice-cold PBS, removed from the plate with a cell scraper, and cells from each set of two 15 cm plates were combined (i.e., cells from the two WT-SOD1

plates were combined, etc.) to a total of three samples. Cells were lysed in 600 µL of TNTE coimmunoprecipitation buffer containing protease inhibitors by gentle rotation at 4 °C for 25 minutes. Following incubation, cells were passaged 10 times through a 25-G needle. Lysates were cleared by centrifugation at 21,000 x g for 10 minutes at 4 °C. Five-hundred microliters of lysate were loaded onto a Superdex 200 10/300 GL size exclusion column and separated and eluted with PBS on an AKTA-Pure FPLC system (GE Healthcare). Lysates were fractionated at a rate of 0.5 mL/min into 48 fractions. Fractions were resolved via SDS PAGE on a 15% gel and immunostained for FLAG and endogenous SOD1.

Mitochondrial Membrane Potential Assay. Mitochondrial membrane potential in cells (same cells as in the Cell Survival Assay, described above) was assayed with the JC-1 Mitochondrial Membrane Potential Assay Kit (Abcam 113850) based on an adaptation of the manufacturer's instructions. Specifically, for each sample, medium was collected and saved in a 12x75 mm polystyrene test tube. Cells were washed once with PBS, which was added to the corresponding test tube. Following the wash, cells were trypsinized and cells were collected into the same tube. Tubes were capped and centrifuged at 1000 x g for 5 minutes. The supernatant was discarded and cells were resuspended in 1 mL of warm complete medium. 10 µL of 200 µM JC-1 in DMSO was then added to each sample. No stain was added to a separate sample, as a control. After addition of stain, the samples were protected from light and incubated at 37 ºC for 20 minutes, followed by a single 2 mL wash with PBS. Cells were resuspended in 500 µL of PBS and analyzed on an Accuri C6 flow cytometer. Emission spectra from excitation at 488 nm were detected with the FL-1 and FL-2 emission filters. Standard compensation was carried out based on control Cas9 cells.

Mitochondrial ROS Determination. The relative number of ROS-containing cells (same cells as in the Cell Survival Assay) was determined by a flow cytometry-based application of MitoSOX Red Mitochondrial Superoxide Indicator (Life Technologies M36008). After cells were grown to 80% confluence in 12-well plates, 10 mM antimycin A was added to the positive control cells to a final concentration of 30 μM and incubated for 40 minutes in a 5% CO_2, 37 ºC incubator. Following incubation, cell medium was collected and saved in a 12x75 mm polystyrene test tube. Cells were washed once with PBS, which was added to the corresponding test tube. Following the wash, cells were trypsinized and cells were collected into the same tube. Tubes were capped and centrifuged at 600 x g for 3 minutes. The supernatant was discarded and cells were washed once in 1 mL of warm complete medium. To stain cells, 5 mM MitoSOX Red was prepared in DMSO as indicated by the manufacturer, which was then diluted to 5 μM in complete medium. All samples were resuspended in 1 mL of the 5 μM MitoSOX-containing medium, except the negative control which was resuspended in 1 mL of complete medium. After addition of stain, the samples were protected from light and incubated for 10 minutes at 37 ºC and 5% CO_2, followed by a 3-minute centrifugation at 600 x g and a single 1 mL PBS wash. Cells were resuspended in 1 mL of PBS and passed through a 70 μm cell strainer, diluted to approximately 500,000 cells/mL, and analyzed on either an Accuri C6 or an Attune Acoustic Focusing Cytometer (Life Technologies). Emission spectra from excitation at 488 nm were detected with the BL-3 or FL-3 emission filter.

Live Cell Confocal Imaging. Cells (same as in the Cell Survival Assay) were seeded at medium density into 35 mm glass bottom microwell dishes (MatTek, P35GC-1.5-10-C) and allowed to adhere for 24 hours. Prior to staining, positive control cells were treated for 40 minutes with 30 μM antimycin A. To stain cells, MitoSOX Red was prepared as in the ROS determination assay, cells were washed once with warm complete medium, and 1 mL of MitoSOX medium was

added to each plate, except the negative control (1 mL complete medium). Cells were incubated protected from light for 10 minutes at 37 ºC and 5% CO_2 atmosphere, after which they were washed 3 x with warm complete medium. Nuclei were counterstained with 1 µg/mL Hoechst 33342 (Pierce 62249) according to manufacturer's protocol, using a 10-minute incubation time, followed by a PBS wash. Cells were then treated for at least 45 minutes with 1 mL of ProLong Live Antifade Reagent, for live cell imaging (Molecular Probes P36975), 1:100 in complete DMEM. Finally, at the time of imaging the plate was transferred to a humidified, 5% CO_2, 37 ºC mini chamber adapted to the microscope stage.

Cells were imaged on a Leica (Buffalo Grove, IL, USA) TCS SP8 HyD using the resonance scanning mode. Images were collected from a 63x oil objective. Data collection parameters were determined based on fluorescence signal from the positive control. Images were oversampled and deconvolved with the Huygens Essential software version 16.10 (Scientific Volume Imaging, The Netherlands, http://svi.nl) after which strong automatic dye separation was applied. All samples and images were treated identically.

Statistical Analysis. Statistical analysis was conducted with either a one-way ANOVA with Tukey's post-hoc test or with an unpaired, equal variance, two-tailed t-test. Where indicated, SEM was determined after normalization of each replicate.

REFERENCES

1. **Cross CE, Halliwell B, Borish ET, et al.** 1987. OXygen radicals and human disease. Annals of Internal Medicine **107:**526-545.

2. **dickinson BC, Chang CJ.** 2011. Chemistry and biology of reactive oxygen species in signaling or stress responses. Nature Chemical Biology **7:**504-511.

3. **Barnham KJ, Masters CL, Bush AI.** 2004. Neurodegenerative diseases and oxidative stress. Nature reviews Drug discovery **3:**205-214.

4. **Finkel T, Serrano M, Blasco MA.** 2007. The common biology of cancer and ageing. Nature **448:**767-774.

5. **Finkel T.** 2011. Signal transduction by reactive oxygen species. The Journal of Cell Biology **194:**7-15.

6. **Corson LB, Strain, J.J., Culotta, V.C. & Cleveland, D.W.** 1998. Chaperone-facilitated copper binding is a property common to several classes of familial amyotrophic lateral sclerosis-linked superoxide dismutase mutants. Proceedings of the National Academy of Sciences of the United States of America **95:**6361-6366.

7. **Tsang C. K. L, Y., Thomas, J., Zhang. Y., Zheng X. F.** 2014. Superoxide dismutase 1 acts as a nuclear transcription factor to regulate oxidative stress resistance. Nat Commun **5:**3446.

8. **Wood LK, Thiele DJ.** 2009. Transcriptional activation in yeast in response to copper deficiency involves copper-zinc superoxide dismutase. J Biol Chem **284:**404-413.

9. **Culotta VC, Joh HD, Lin SJ, Slekar KH, Strain J.** 1995. A physiological role for *Saccharomyces cerevisiae* copper/zinc superoxide dismutase in copper buffering. J Biol Chem **270:**29991-29997.

10. **Wei JP, Srinivasan C, Han H, Valentine JS, Gralla EB.** 2001. Evidence for a novel role of copper-zinc superoxide dismutase in zinc metabolism. J Biol Chem **276:**44798-44803.

11. **Cobine PA, Pierrel F, Bestwick ML, Winge DR.** 2006. Mitochondrial Matrix Copper Complex Used in Metallation of Cytochrome Oxidase and Superoxide Dismutase. Journal of Biological Chemistry **281:**36552-36559.

12. **Khalimonchuk O, Winge DR.** 2008. Function and redox state of mitochondrial localized cysteine-rich proteins important in the assembly of cytochrome c oxidase. Biochimica et biophysica acta **1783:**618-628.

13. **Reddi AR, Culotta VC.** 2013. SOD1 integrates signals from oxygen and glucose to repress respiration. Cell **152:**224-235.

14. **Rosen DR, Siddique T, Patterson D, Figlewicz DA, Sapp P, Hentati A, Donaldson D, Goto J, O'Regan JP, Deng H-X, Rahmani Z, Krizus A, McKenna-Yasek D, Cayabyab A, Gaston SM, Berger R, Tanzi RE, Halperin JJ, Herzfeldt B, Van den Bergh R, Hung W-Y, Bird T, Deng G, Mulder DW, Smyth C, Laing NG, Soriano E, Pericak-Vance MA, Haines J, Rouleau GA, Gusella JS, Horvitz HR, Brown RH.** 1993. Mutations in Cu/Zn superoxide dismutase gene are associated with familial amyotrophic lateral sclerosis. Nature **362:**59-62.

15. **Deng H-X, Hentati A, Tainer JA, Iqbal Z, Cayabyab A, Hung W-Y, Getzoff ED, Hu P, Herzfeldt B, Roos RP, Warner C, Deng G, Soriano E, Smyth C, Parge HE, Ahmed A, Roses AD, Hallewell RA, Pericak-Vance MA, Siddique T.** 1993. Amyotrophic Lateral Sclerosis and Structural Defects in Cu,Zn Superoxide Dismutase. Science **261:**1047-1051.

16. **Chio A, Traynor BJ, Lombardo F, Fimognari M, Calvo A, Ghiglione P, Mutani R, Restagno G.** 2008. Prevalence of SOD1 mutations in the Italian ALS population. Neurology **70:**533-537.

17. **Zhang F, Zhu H.** 2006. Intracellular conformational alterations of mutant SOD1 and the implications for fALS-associated SOD1 mutant induced motor neuron cell death. Biochimica et Biophysica Acta (BBA) - General Subjects **1760:**404-414.

18. **Sreedharan J, Brown RH.** 2013. Amyotrophic lateral sclerosis: Problems and prospects. Annals of Neurology **74:**309-316.

19. **Münch C, Bertolotti A.** 2010. Exposure of Hydrophobic Surfaces Initiates Aggregation of Diverse ALS-Causing Superoxide Dismutase-1 Mutants. Journal of Molecular Biology **399:**512-525.

20. **Elam JS, Taylor AB, Strange R, Antonyuk S, Doucette PA, Rodriguez JA, Hasnain SS, Hayward LJ, Valentine JS, Yeates TO, Hart PJ.** 2003. Amyloid-like filaments and water-filled nanotubes formed by SOD1 mutant proteins linked to familial ALS. Nat Struct Mol Biol **10:**461-467.

21. **Tiwari A, Liba A, Sohn SH, Seetharaman SV, Bilsel O, Matthews CR, Hart PJ, Valentine JS, Hayward LJ.** 2009. Metal Deficiency Increases Aberrant Hydrophobicity of Mutant Superoxide Dismutases That Cause Amyotrophic Lateral Sclerosis. The Journal of Biological Chemistry **284:**27746-27758.

22. **Choi I, In Yang Y, Song HD, Lee JS, Kang T, Sung J-J, Yi J.** 2011. Lipid molecules induce the cytotoxic aggregation of Cu/Zn superoxide dismutase with structurally disordered regions. Biochimica et Biophysica Acta (BBA) - Molecular Basis of Disease **1812:**41-48.

23. **Abdolvahabi A, Shi Y, Rhodes NR, Cook NP, Marti AA, Shaw BF.** 2015. Arresting amyloid with coulomb's law: acetylation of ALS-linked SOD1 by aspirin impedes aggregation. Biophys J **108:**1199-1212.

24. **Pickles S, Destroismaisons L, Peyrard SL, Cadot S, Rouleau GA, Brown RH, Julien J-P, Arbour N, Velde CV.** 2013. Mitochondrial damage revealed by immunoselection for ALS-linked misfolded SOD1. Human molecular genetics **22:**3947-3959.

25. **Zhang F, Ström A-L, Fukada K, Lee S, Hayward LJ, Zhu H.** 2007. Interaction between Familial Amyotrophic Lateral Sclerosis (ALS)-linked SOD1 Mutants and the Dynein Complex. Journal of Biological Chemistry **282:**16691-16699.

26. **Somwar R, Erdjument-Bromage H, Larsson E, Shum D, Lockwood WW, Yang G, Sander C, Ouerfelli O, Tempst PJ, Djaballah H, Varmus HE.** 2011. Superoxide dismutase 1 (SOD1) is a target for a small molecule identified in a screen for inhibitors of the growth of lung adenocarcinoma cell lines. Proceedings of the National Academy of Sciences **108:**16375-16380.

27. **Glasauer A, Sena LA, Diebold LP, Mazar AP, Chandel NS.** 2014. Targeting SOD1 reduces experimental non-small-cell lung cancer. J Clin Invest **124:**117-128.

28. **Papa L, Hahn, M., Marsh, E.L., Evans, B.S. & Germain, D.** 2014. SOD2 to SOD1 switch in breast cancer. Journal of Biological Chemistry **289:**5412-5416.

29. **Liou G-Y, Storz P.** 2010. Reactive oxygen species in cancer. Free radical research **44:**10.3109/10715761003667554.

30. **Sullivan LB, Chandel NS.** 2014. Mitochondrial reactive oxygen species and cancer. Cancer & Metabolism **2:**17.

31. **Choudhary C, Kumar C, Gnad F, Nielsen ML, Rehman M, Walther TC, Olsen JV, Mann M.** 2009. Lysine acetylation targets protein complexes and co-regulates major cellular functions. Science **325:**834-840.

32. **Ciriolo MR, Battistoni A, Falconi M, Filomeni G, Rotilio G.** 2001. Role of the electrostatic loop of Cu,Zn superoxide dismutase in the copper uptake process. European Journal of Biochemistry **268:**737-742.

33. **Banci L, Bertini I, Cantini F, D'Amelio N, Gaggelli E.** 2006. Human SOD1 before Harboring the Catalytic Metal: SOLUTION STRUCTURE OF COPPER-DEPLETED, DISULFIDE-REDUCED FORM. Journal of Biological Chemistry **281:**2333-2337.

34. **Perry JJP, Shin DS, Getzoff ED, Tainer JA.** 2010. The structural biochemistry of the superoxide dismutases. Biochimica et biophysica acta **1804:**245-262.

35. **Andersen JL, Thompson JW, Lindblom KR, Johnson ES, Yang CS, Lilley LR, Freel CD, Moseley MA, Kornbluth S.** 2011. A biotin switch-based proteomics approach identifies 14-3-3zeta as a target of Sirt1 in the metabolic regulation of caspase-2. Molecular Cell **43:**834-842.

36. **Park J, Chen Y, Tishkoff DX, Peng C, Tan M, Dai L, Xie Z, Zhang Y, Zwaans BMM, Skinner ME, Lombard DB, Zhao Y.** 2013. SIRT5-Mediated Lysine Desuccinylation Impacts Diverse Metabolic Pathways. Molecular cell **50:**919-930.

37. **Lin Z, Xu, H., Wang, J., Lin, Q., Ruan, Z., Liu, F., Jin, W., Huang, H. & Chen, X.** 2013. SIRT5 desuccinylates and activates SOD1 to eliminate ROS. Biochemical and Biophysical Research Communications **441:**191-195.

38. **Dewhurst HM, Torres MP.** 2017. Systematic analysis of non-structural protein features for the prediction of PTM function potential by artificial neural networks. PLoS One **12:**e0172572.

39. **Torres MP, Dewhurst H, Sundararaman N.** 2016. Proteome-wide Structural Analysis of PTM Hotspots Reveals Regulatory Elements Predicted to Impact Biological Function and Disease. Mol Cell Proteomics **15:**3513-3528.

40. **McCord JM, Fridovich I.** 1969. Superoxide dismutase: An enzymic function for erythrocuprein (hemocuprein). J Biol Chem **244:**6049-6055.

41. **Reddi AR, Jensen LT, Naranuntarat A, Rosenfeld L, Leung E, Shah R, Culotta VC.** 2009. The overlapping roles of manganese and Cu/Zn SOD in oxidative stress protection. Free Radic Biol Med **46:**154-162.

42. **Sanchez RJ, Srinivasan C, Munroe WH, Wallace MA, Martins J, Kao TY, Le K, Gralla EB, Valentine JS.** 2005. Exogenous manganous ion at millimolar levels rescues all known dioxygen-sensitive phenotypes of yeast lacking CuZnSOD. J Biol Inorg Chem **10:**913-923.

43. **Elchuri S, Oberley TD, Qi W, Eisenstein RS, Jackson Roberts L, Van Remmen H, Epstein CJ, Huang TT.** 2005. CuZnSOD deficiency leads to persistent and widespread oxidative damage and hepatocarcinogenesis later in life. Oncogene **24:**367-380.

44. **Blander G, de Oliveira RM, Conboy CM, Haigis M, Guarente L.** 2003. Superoxide dismutase 1 knock-down induces senescence in human fibroblasts. J Biol Chem **278:**38966-38969.

45. **Phillips J, Campbell S, Michard D, Charbonneau M, Hilliker A.** 1989. Null mutations of copper/zinc superoxide in Drosophila confer hypersensitivity to paraquat and reduced longevity. Proc Natl Acad Sci USA **83:**3820-3824.

46. **Corson LB, Folmer J, Strain JS, Culotta VC, Cleveland DW.** 1999. Oxidative stress and iron are implicated in fragmenting vacuoles of *Saccharomyces cerevisiae* lacking Cu,Zn Superoxide dismtuase. J Biol Chem **274:**27590-27596.

47. **McNaughton RL, Reddi AR, Clement MH, Sharma A, Barnese K, Rosenfeld L, Gralla EB, Valentine JS, Culotta VC, Hoffman BM.** 2010. Probing in vivo Mn2+ speciation and oxidative stress resistance in yeast cells with electron-nuclear double resonance spectroscopy. Proc Natl Acad Sci U S A **107:**15335-15339.

48. **Papa L, Manfredi G, Germain D.** 2014. SOD1, an unexpected novel target for cancer therapy. Genes Cancer **5:**15-21.

49. **Palomo GM, Manfredi G.** 2015. Exploring new pathways of neurodegeneration in ALS: the role of mitochondria quality control. Brain Res **1607:**36-46.

50. **De Freitas JM, Liba A, Meneghini R, Valentine JS, Gralla EB.** 2000. Yeast lacking Cu-Zn superoxide dismutase show altered iron homeostasis. Role of oxidative stress in iron metabolism. J Biol Chem **275:**11645-11649.

51. **Inoue E, Tano K, Yoshii H, Nakamura J, Tada S, Watanabe M, Seki M, Enomoto T.** 2010. SOD1 Is Essential for the Viability of DT40 Cells and Nuclear SOD1 Functions as a Guardian of Genomic DNA. J Nucleic Acids **2010**.

52. **Mortenson JB, Heppler LN, Banks CJ, Weerasekara VK, Whited MD, Piccolo SR, Johnson WE, Thompson JW, Andersen JL.** 2015. Histone deacetylase 6 (HDAC6) promotes the pro-survival activity of 14-3-3zeta via deacetylation of lysines within the 14-3-3zeta binding pocket. J Biol Chem.

53. **Dewhurst HM, Choudhury S, Torres MP.** 2015. Structural Analysis of PTM Hotspots (SAPH-ire)--A Quantitative Informatics Method Enabling the Discovery of Novel Regulatory Elements in Protein Families. Mol Cell Proteomics **14:**2285-2297.

54. **R. Rakhit AC.** 2006. Structure, folding, and misfolding of Cu,Zn superoxide dismutase in amyotrophic lateral sclerosis. Biochimica et Biophysica Acta (BBA) **1762:**1025-1037.

55. **Weinert BT, Scholz C, Wagner SA, Iesmantavicius V, Su D, Daniel JA, Choudhary C.** 2013. Lysine succinylation is a frequently occurring modification in prokaryotes and eukaryotes and extensively overlaps with acetylation. Cell Rep **4:**842-851.

56. **Lin C, Zeng H, Lu J, Xie Z, Sun W, Luo C, Ding J, Yuan S, Geng M, Huang M.** 2015. Acetylation at lysine 71 inactivates superoxide dismutase 1 and sensitizes cancer cells to genotoxic agents. Oncotarget **6:**20578-20591.

57. **Zhao S, Xu W, Jiang W, Yu W, Lin Y, Zhang T, Yao J, Zhou L, Zeng Y, Li H, Li Y, Shi J, An W, Hancock SM, He F, Qin L, Chin J, Yang P, Chen X, Lei Q, Xiong Y, Guan KL.** 2010. Regulation of cellular metabolism by protein lysine acetylation. Science **327:**1000-1004.

58. **Kaliszewski M, Kennedy AK, Blaes SL, Shaffer RS, Knott AB, Song W, Hauser HA, Bossy B, Huang TT, Bossy-Wetzel E.** 2016. SOD1 Lysine 123 Acetylation in the Adult Central Nervous System. Front Cell Neurosci **10:**287.

59. **Xiong Y, Guan KL.** 2012. Mechanistic insights into the regulation of metabolic enzymes by acetylation. J Cell Biol **198:**155-164.

60. **Hirschey MD, Zhao Y.** 2015. Metabolic Regulation by Lysine Malonylation, Succinylation, and Glutarylation. Mol Cell Proteomics **14:**2308-2315.

61. **Du J, Zhou Y, Su X, Yu JJ, Khan S, Jiang H, Kim J, Woo J, Kim JH, Choi BH, He B, Chen W, Zhang S, Cerione RA, Auwerx J, Hao Q, Lin H.** 2011. Sirt5 is a NAD-dependent protein lysine demalonylase and desuccinylase. Science **334:**806-809.

62. **Nishida Y, Rardin, M.J., Carrico, C., He, W., Sahu, A.K., Gut, P., Najjar, R., Fitch, M., Hellerstein, M., Gibson, B.W. & Verdin, E.** 2015. SIRT5 Regulates both Cytosolic

and Mitochondrial Protein Malonylation with Glycolysis as a Major Target. Molecular Cell **59:**321-332.

63. **Matsushita N, Yonashiro, R., Ogata, Y. Sugiura, A., Nagashima, S., Fukuda, T., Inatome, R. & Yanagi, S.** 2011. Distinct regulation of mitochondrial localization and stability of two human Sirt5 isoforms. Genes to cells: devoted to molecular & cellular mechanisms **16:**190-202.

64. **Rardin MJ, He, W., Nishida, Y., Newman, J.C., Carrico, C., Danielson, S.R., Guo, A., Gut, P., Sahu, A.K., Li, Biao, Uppala, R., Fitch, M., Riiff, T., Zhu, L., Zhou, J., Mulhern, D., Stevens, R.D., Ilkayeva, O.R., Newgard, C.B., Jacobson, M.P., Hellerstein, M., Goetzman, E.S., Gibson, B.W. & Verdin, E.** 2013. SIRT5 Regulates the Mitochondrial Lysine Succinylome and Metabolic Networks. Cell Metabolism **18:**920-933.

65. **Vijayvergiya C, Beal, M.F., Buck, J. & Manfredi, G.** 2005. Mutant Superoxide Dismutase 1 Forms Aggregates in the Brain Mitochondrial Matrix of Amyotrophic Lateral Sclerosis Mice. Journal of Neuroscience **25:**2463-2470.

66. **Magrane J, Hervias I, Henning MS, Damiano M, Kawamata H, Manfredi G.** 2009. Mutant SOD1 in neuronal mitochondria causes toxicity and mitochondrial dynamics abnormalities. Hum Mol Genet **18:**4552-4564.

67. **Kawamata H, Manfredi G.** 2010. Import, maturation, and function of SOD1 and its copper chaperone CCS in the mitochondrial intermembrane space. Antioxid Redox Signal **13:**1375-1384.

68. **Kawamata HM, G.** 2010. Import, Maturation, and Function of SOD1 and Its Copper Chaperone in the Mitochondrial Intermembrane Space. Antioxidants & Redox Signaling **13:**1375-1384.

69. **Bihlmaier K, Mesecke, N., Terziyska, N., Bien, M., Hell, K. & Herrmann, J.M.** 2007. The disulfide relay system of mitochondria is connected to the respiratory chain. Journal of Cell Biology **179:**389-395.

70. **Takeshige K, Minakami S.** 1979. NADH- and NADPH-dependent formation of superoxide anions by bovine heart submitochondrial particles and NADH-ubiquinone reductase preparation. Biochem J **180:**129-135.

71. **Raha S, Robinson BH.** 2000. Mitochondria, oxygen free radicals, disease and ageing. Trends Biochem Sci **25:**502-508.

72. **Fischer LR, Igoudjil A, Magrane J, Li Y, Hansen JM, Manfredi G, Glass JD.** 2011. SOD1 targeted to the mitochondrial intermembrane space prevents motor neuropathy in the Sod1 knockout mouse. Brain **134:**196-209.

73. **Sturtz LA, Diekert K, Jensen LT, Lill R, Culotta VC.** 2001. A fraction of yeast Cu,Zn-superoxide dismutase and its metallochaperone, CCS, localize to the intermembrane

space of mitochondria. A physiological role for SOD1 in guarding against mitochondrial oxidative damage. J Biol Chem **276:**38084-38089.

74. **Kawamata H, Manfredi G.** 2008. Different regulation of wild-type and mutant Cu,Zn superoxide dismutase localization in mammalian mitochondria. Hum Mol Genet **17:**3303-3317.

75. **Reddehase S, Grumbt B, Neupert W, Hell K.** 2009. The disulfide relay system of mitochondria is required for the biogenesis of mitochondrial Ccs1 and Sod1. J Mol Biol **385:**331-338.

76. **Jacobson J, Duchen MR, Hothersall J, Clark JB, Heales SJ.** 2005. Induction of mitochondrial oxidative stress in astrocytes by nitric oxide precedes disruption of energy metabolism. J Neurochem **95:**388-395.

77. **Zorov DB, Juhaszova M, Sollott SJ.** 2014. Mitochondrial reactive oxygen species (ROS) and ROS-induced ROS release. Physiol Rev **94:**909-950.

78. **Longo VD, Gralla EB, Valentine JS.** 1996. Superoxide dismutase activity is essential for stationary phase survival in Saccharomyces cerevisiae. Mitochondrial production of toxic oxygen species in vivo. J Biol Chem **271:**12275-12280.

79. **Kelly B, Tannahill GM, Murphy MP, O'Neill LA.** 2015. Metformin Inhibits the Production of Reactive Oxygen Species from NADH:Ubiquinone Oxidoreductase to Limit Induction of Interleukin-1beta (IL-1beta) and Boosts Interleukin-10 (IL-10) in Lipopolysaccharide (LPS)-activated Macrophages. J Biol Chem **290:**20348-20359.

80. **Ouslimani N, Peynet J, Bonnefont-Rousselot D, Therond P, Legrand A, Beaudeux JL.** 2005. Metformin decreases intracellular production of reactive oxygen species in aortic endothelial cells. Metabolism **54:**829-834.

81. **Marycz K, Tomaszewski KA, Kornicka K, Henry BM, Wronski S, Tarasiuk J, Maredziak M.** 2016. Metformin Decreases Reactive Oxygen Species, Enhances Osteogenic Properties of Adipose-Derived Multipotent Mesenchymal Stem Cells In Vitro, and Increases Bone Density In Vivo. Oxid Med Cell Longev **2016:**9785890.

82. **Lenaz G, Fato R, Genova ML, Bergamini C, Bianchi C, Biondi A.** 2006. Mitochondrial Complex I: structural and functional aspects. Biochim Biophys Acta **1757:**1406-1420.

83. **Levine B, Mizushima N, Virgin HW.** 2011. Autophagy in immunity and inflammation. Nature **469:**323-335.

84. **Kroemer G, Mariño G, Levine B.** 2010. Autophagy and the Integrated Stress Response. Molecular Cell **40:**280-293.

85. **Lilienbaum A.** 2013. Relationship between the proteasomal system and autophagy. International Journal of Biochemistry and Molecular Biology **4:**1-26.

86. **Lynch-Day MA, Mao K, Wang K, Zhao M, Klionsky DJ.** 2012. The Role of Autophagy in Parkinson's Disease. Cold Spring Harbor Perspectives in Medicine **2**.

87. **Wang B, Abraham N, Gao G, Yang Q.** 2016. Dysregulation of autophagy and mitochondrial function in Parkinson's disease. Translational Neurodegeneration **5:**19.

88. **Arrasate M, Finkbeiner S.** 2012. Protein aggregates in Huntington's disease. Experimental neurology **238:**1-11.

89. **Zare-shahabadi A, Masliah E, Johnson GVW, Rezaei N.** 2015. Autophagy in Alzheimer's Disease. Reviews in the neurosciences **26:**385-395.

90. **Lee JK, Shin JH, Lee JE, Choi E-J.** 2015. Role of autophagy in the pathogenesis of amyotrophic lateral sclerosis. Biochimica et Biophysica Acta (BBA) - Molecular Basis of Disease **1852:**2517-2524.

91. **Levine B, Kroemer G.** 2008. Autophagy in the Pathogenesis of Disease. Cell **132:**27-42.

92. **Mizushima N, Yoshimori T, Levine B.** 2010. Methods in Mammalian Autophagy Research. Cell **140:**313-326.

93. **Tanida I, Ueno T, Kominami E.** 2008. LC3 and Autophagy, p 77-88. *In* Deretic V (ed), Autophagosome and Phagosome. Humana Press, Totowa, NJ.

94. **Weerasekara VK, Panek DJ, Broadbent DG, Mortenson JB, Mathis AD, Logan GN, Prince JT, Thomson DM, Thompson JW, Andersen JL.** 2014. Metabolic-Stress-Induced Rearrangement of the 14-3-3ζ Interactome Promotes Autophagy via a ULK1- and AMPK-Regulated 14-3-3ζ Interaction with Phosphorylated Atg9. Molecular and Cellular Biology **34:**4379-4388.

95. **Yang Y-p, Hu L-f, Zheng H-f, Mao C-j, Hu W-d, Xiong K-p, Wang F, Liu C-f.** 2013. Application and interpretation of current autophagy inhibitors and activators. Acta Pharmacol Sin **34:**625-635.

96. **Sargsyan A, Cai J, Fandino LB, Labasky ME, Forostyan T, Colosimo LK, Thompson SJ, Graham TE.** 2015. Rapid parallel measurements of macroautophagy and mitophagy in mammalian cells using a single fluorescent biosensor. **5:**12397.

97. **Davies MN, Kjalarsdottir L, Thompson JW, Dubois LG, Stevens RD, Ilkayeva OR, Brosnan MJ, Rolph TP, Grimsrud PA, Muoio DM.** 2016. The Acetyl Group Buffering Action of Carnitine Acetyltransferase Offsets Macronutrient-Induced Lysine Acetylation of Mitochondrial Proteins. Cell Rep **14:**243-254.

98. **Kulej K, Avgousti DC, Sidoli S, Herrmann C, Della Fera AN, Kim ET, Garcia BA, Weitzman MD.** 2017. Time-resolved global and chromatin proteomics during herpes simplex virus (HSV-1) infection. Mol Cell Proteomics.

99. **Soderblom EJ, Philipp M, Thompson JW, Caron MG, Moseley MA.** 2011. Quantitative label-free phosphoproteomics strategy for multifaceted experimental designs. Analytical Chemistry **83:**3758-3764.

100. **Hoos MD, Richardson BM, Foster MW, Everhart A, Thompson JW, Moseley MA, Colton CA.** 2013. Longitudinal study of differential protein expression in an Alzheimer's mouse model lacking inducible nitric oxide synthase. J Proteome Res **12:**4462-4477.

101. **Finn RD, Bateman A, Clements J, Coggill P, Eberhardt RY, Eddy SR, Heger A, Hetherington K, Holm L, Mistry J, Sonnhammer EL, Tate J, Punta M.** 2014. Pfam: the protein families database. Nucleic Acids Res **42:**D222-230.

102. **Edgar RC.** 2004. MUSCLE: a multiple sequence alignment method with reduced time and space complexity. BMC Bioinformatics **5:**113.

103. **Tighe A, Johnson VL, Taylor SS.** 2004. Truncating APC mutations have dominant effects on proliferation, spindle checkpoint control, survival and chromosome stability. J Cell Sci **117:**6339-6353.

104. **Goto H, Inagaki M.** 2007. Production of a site- and phosphorylation state-specific antibody. Nat Protoc **2:**2574-2581.

105. **Flohe L, Otting F.** 1984. Superoxide dismutase assays. Methods Enzymol **105:**93-104.

106. **Ran FA, Hsu PD, Wright J, Agarwala V, Scott DA, Zhang F.** 2013. Genome engineering using the CRISPR-Cas9 system. Nat Protoc **8:**2281-2308.

107. **Hodson AE, Tippetts TS, Bikman BT.** 2015. Insulin treatment increases myocardial ceramide accumulation and disrupts cardiometabolic function. Cardiovasc Diabetol **14:**153.

108. **Wisniewski JR, Zougman A, Nagaraj N, Mann M.** 2009. Universal sample preparation method for proteome analysis. Nat Meth **6:**359-362.

109. **Naylor BC, Porter MT, Wilson E, Herring A, Lofthouse S, Hannemann A, Piccolo SR, Rockwood AL, Price JC.** 2017. DeuteRater: a tool for quantifying peptide isotope precision and kinetic proteomics. Bioinformatics **33:**1514-1520.

110. **Polpitiya AD, Qian W-J, Jaitly N, Petyuk VA, Adkins JN, Camp DG, Anderson GA, Smith RD.** 2008. DAnTE: a statistical tool for quantitative analysis of -omics data. Bioinformatics (Oxford, England) **24:**1556-1558.

111. **Babicki S, Arndt D, Marcu A, Liang Y, Grant JR, Maciejewski A, Wishart DS.** 2016. Heatmapper: web-enabled heat mapping for all. Nucleic Acids Research **44:**W147-W153.